California Department of Fish and Wildlife
Stream Evaluation Report 2026-01

INSTREAM FLOW EVALUATION: CLEAR LAKE HITCH PASSAGE IN TRIBUTARIES OF THE CLEAR LAKE WATERSHED, LAKE COUNTY

APPENDICES

TABLE OF CONTENTS

ABBREVIATIONS AND ACRONYMS

AOI	area of interest
2D	two-dimensional (physical habitat simulation model)
CDFW	California Department of Fish and Wildlife (previously CDFG)
CLH	Clear Lake Hitch
cfs	cubic feet per second
D_{50}	particle diameter at 50% or the median particle size
DEM	digital elevation model
DSA(s)	depth sensitive area(s)
ft	foot/feet
ft/s	feet per second
HEC-RAS	Hydrologic Engineering Center's River Analysis System
lidar	light detection and ranging
MDSA (s)	most depth sensitive area(s)
NIR	near-infrared
mm	millimeters
nm	nanometers
RTK-GPS	Real Time Kinematic Global Positioning System
SOP	standard operating procedure
SWE-ELM	Shallow Water Equations – Eulerian-Lagrangian Method
TIN	triangulated irregular network
USFWS	United States Fish and Wildlife Service
U.S.	United States
WSE	water surface elevation

APPENDIX A: LIGHT DETECTION AND RANGING DATA

A.1 Introduction

The California Department of Fish and Wildlife (CDFW) developed two-dimensional (2D) hydraulic habitat models to identify minimum flows needed for Clear Lake Hitch (CLH) passage in tributaries of the Clear Lake watershed. The 2D module of the U.S. Army Corps of Engineers Hydrologic Engineering Center's River Analysis System (HEC-RAS) software was used to develop each study tributary 2D model (USACE 2025). A critical input for each tributary model is a digital representation of the terrain surface, or bare-earth digital elevation model (DEM; also referred to as a topobathymetric DEM). CDFW contracted NV5 (Corvallis, Oregon) to acquire high-resolution airborne light detection and ranging (lidar) data and 3-band digital orthoimagery in the six study tributaries surrounding Clear Lake: Adobe, Cole, Kelsey, Manning, Middle, and Scotts creeks (Figure A-1). The purple shading in Figure A-1 illustrates the area of interest (AOI), the defined area where the lidar acquisition, the collection of raw lidar data measurements, occurred for each study tributary. The extent of the AOI was determined with input from Clear Lake Hitch Task Force. The topographic and bathymetric elevation data from the airborne lidar flights were used to develop the DEM needed for each model.

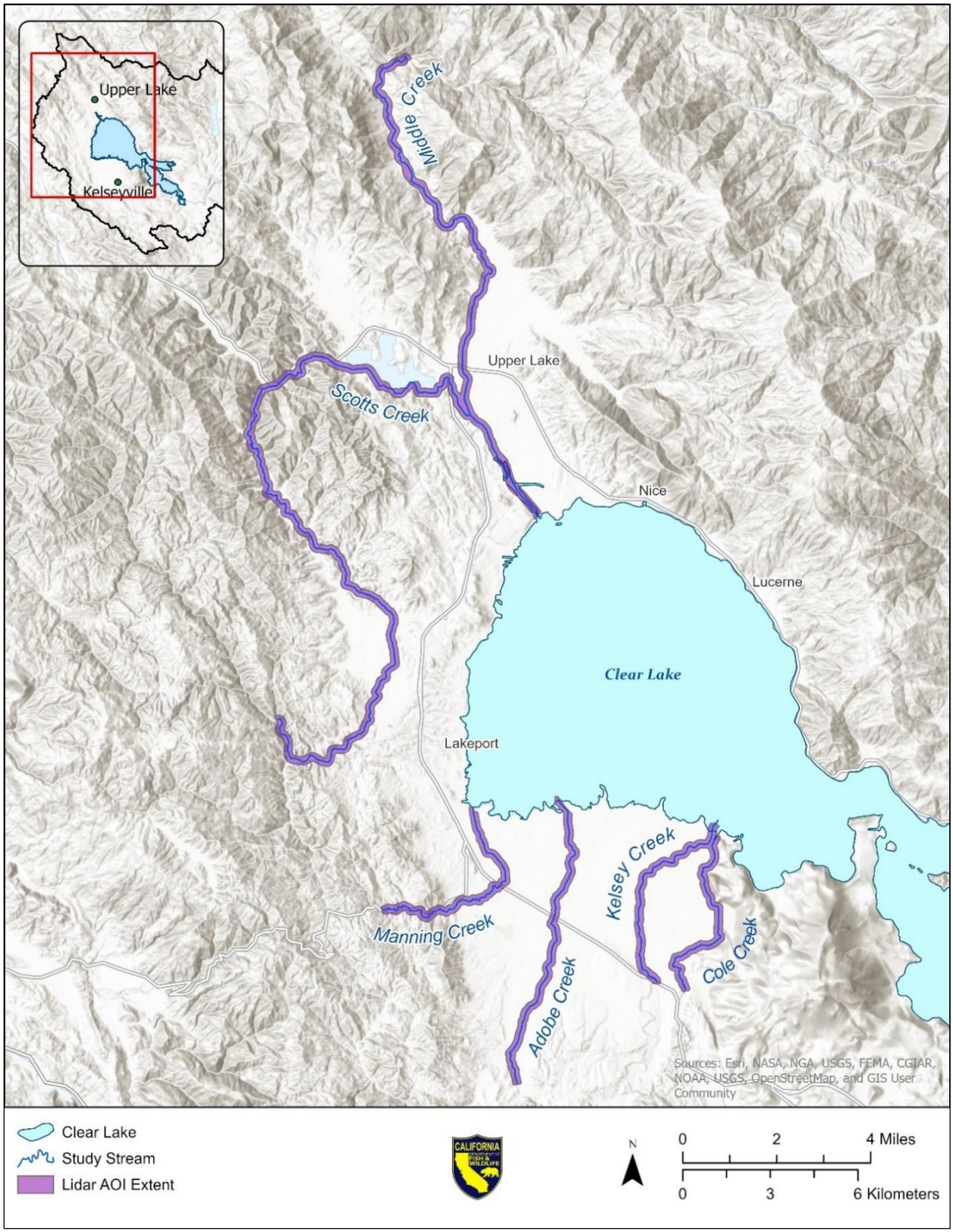

Figure A-1. Map illustrates the area of interest, in purple, that was used for lidar data acquisition in each of the study tributaries.

Airborne lidar is an active remote sensing method in which sensors on an aircraft measure the time of flight for emitted laser light pulses to reach reflective surfaces (e.g., the ground or vegetation) and return to the detector on the aircraft (Kinzel et al. 2012). Distances to the surfaces are calculated from the pulse return travel times and, in combination with information about the aircraft sensor's position and orientation, are used to create a georeferenced, three-dimensional point cloud that serves as the basis of the DEM. Two types of lidar sensors are commonly used, each emitting different laser pulse wavelengths. The standard sensor used for topographic lidar data collection emits near-infrared (NIR) wavelength pulses (λ=1064 nm), which is helpful for capturing streambanks, dry areas, and exposed substrate within the channel. However, NIR pulses are generally absorbed by the water surface, resulting in data voids or inaccurate data in submerged (i.e., wet) stream areas that are important to assess in this study. Bathymetric lidar sensors emit green wavelength laser pulses (λ=532 nm) to capture beneath the water's surface, although may be limited due to water depth, turbidity of the water, and streambed surface reflectivity. NV5 used both NIR and green wavelength sensors to accurately represent the topobathymetric surface.

Lidar acquisition typically covers a larger spatial extent compared to traditional surveying while still producing a highly accurate, high-density grid of georeferenced survey points. During post-processing, the lidar points are classified by laser pulse return type, including default, ground, bathymetric bottom, water surface, or water column (Figure A-2). For this study, NV5 assigned the default point classifications to anthropogenic features such as bridges and vegetation, as seen on the right side of the water column in Figure A-2. NV5 used the classified ground and bathymetric bottom points to produce the DEM.

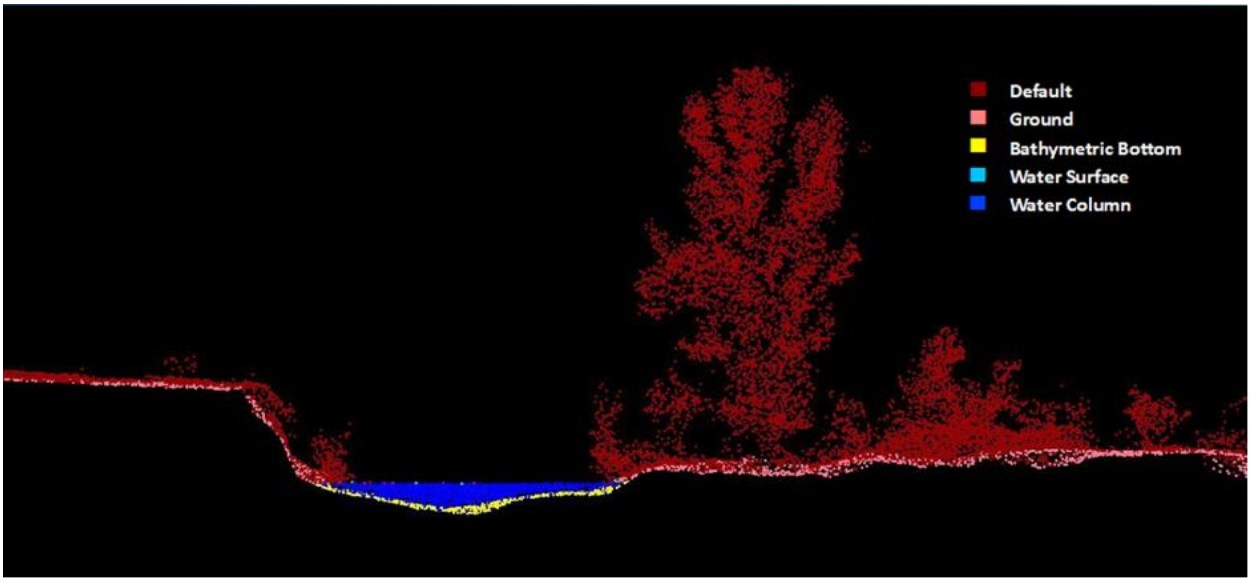

Figure A-2. Example of lidar point cloud data in a cross-sectional view of Kelsey Creek with points classified by laser pulse return type (NV5 2024).

A.2 Planning

CDFW met with NV5 to discuss the AOI and create a specialized plan for the lidar data acquisition. NV5 adjusted lidar acquisition parameters such as flight altitude, laser pulse rate, and laser scan angle to optimize flight paths and meet the target point density of ≥0.74 points/ft^2 (≥ 8 points/m^2). NV5 also considered the availability of satellite constellations, suitable weather, and the best timing for lidar flights due to environmental factors such as water clarity and vegetation growth. High streamflow in winter and early spring can reduce water clarity (increase turbidity) and limit the number of laser pulses that penetrate the water column, while vegetation growth in late spring can block laser penetration to the ground or channel bed. To minimize these impacts, NV5 predicted April as the best time to complete the lidar acquisition.

A.3 Acquisition

NV5 acquired the lidar data from April 6th–April 8th, 2024, using NIR and green wavelength sensors mounted on a Riegl VQ-880-GII laser platform in a Cessna Grand Caravan aircraft. Simultaneously, the digital imagery was collected with a PhaseOne iXM-RS150F medium-format digital camera, which captured the red, green, and blue spectral bands. NV5 established a ground control point network to assist with accuracy assessments and to provide geospatial corrections to help determine the precise position of the aircraft's lidar sensors. NV5 measured turbidity and Secchi depth to understand water clarity conditions prior to and during the lidar data collection at nine locations throughout the AOI.

A.4 Processing

NV5 processed the data using a combination of manual and automated methods. Some of these processing tasks included GPS control computations, best estimate trajectory calculations, kinematic corrections, and classification of the lidar point data (NV5 2024). NV5 used Riegl's RiProcess, a processing software package developed by the lidar sensor manufacturer, to help process and identify the bathymetric (subsurface) returns. After identifying the bathymetric returns, their spatial position had to be corrected since the incident green lidar laser pulses are refracted as they pass through the water column. NV5 used proprietary software, based on Snell's Law, to process the refraction corrections. Where environmental factors (e.g., vegetation) or physical obstructions (e.g., bridges) limited the lidar's penetration, hereinafter referred to as voids, NV5 interpolated the terrain by using the nearest available lidar point data from the area surrounding each void. CDFW used the same control point network established by NV5 to conduct additional topobathymetric surveys with total station and real-time kinematic global positioning system (RTK-GPS). These surveys were needed to more accurately represent the terrain surface in select voids. More information about the additional topographic surveys to fill in lidar voids can be found in Appendix B.

A.5 Results

NV5 acquired roughly 54 miles of lidar data across the six study tributaries, covering approximately 5,942 acres. From these data, NV5 produced a classified lidar point cloud and the lidar-derived DEM that CDFW used to develop the 2D hydraulic habitat models to assess CLH upstream passage. NV5 evaluated the classified, average lidar point densities in the successfully mapped portions of the AOI and found density values of 3.06 points/ft^2 (32.97 points/m^2) for first returns, 1.14 points/ft^2 (12.27 points/m^2) for ground and bathymetric bottom returns, and 1.03 points/ft^2 (11.09 points/m^2) for only bathymetric bottom returns. The void areas lacking bathymetric bottom returns were not used to calculate the average point density value. In this study, the average density of ground surface returns was influenced by the terrain, vegetated canopy cover, and ground surface reflectivity, while the density of bathymetric bottom returns was impacted by depth, turbidity, and stream bottom surface reflectivity (NV5 2024).

NV5 used the classified ground and bathymetric bottom lidar returns to construct a georeferenced DEM (in raster format), which is a digital representation of the topographic and bathymetric elevation surface (Figure A-3). The DEM has an equal-area cell size (resolution) of 1.5 ft and covers the extent of the AOI, including the void-interpolated areas. NV5 delivered both products in units of U.S. survey feet, referenced to the California Coordinate

System of 1983 (2011) epoch 2022.50, and the North American Vertical Datum of 1988, Geoid 18.

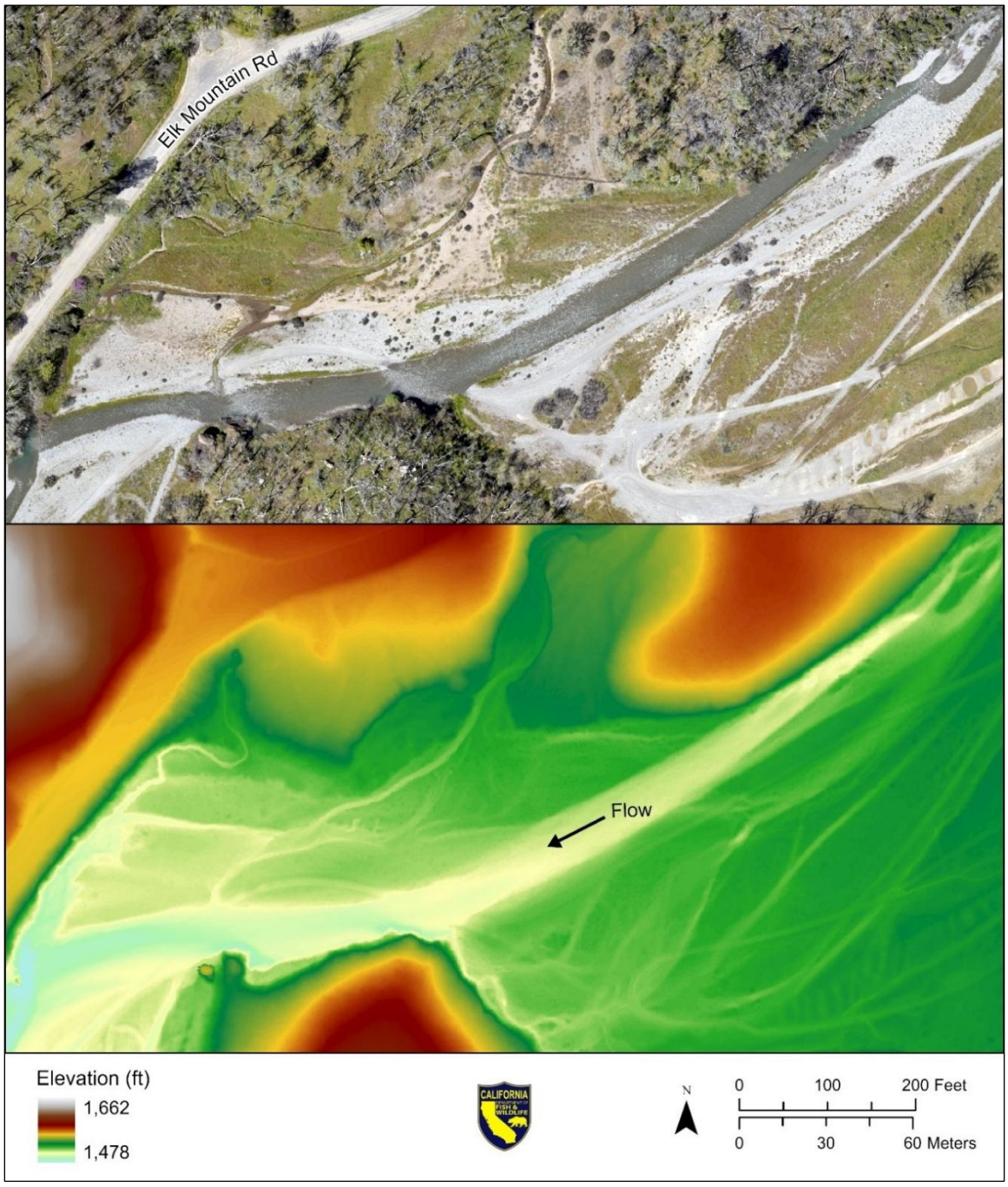

Figure A-3. Comparison between orthoimagery (top) and the lidar-derived digital elevation model (bottom) on a section of upper Middle Creek near the Middle Creek campground.

For questions about the acquisition of lidar data to support this study, please contact instreamflow@wildlife.ca.gov.

APPENDIX B: TOPOGRAPHIC SURVEYING TO FILL LIDAR VOIDS

B.1 Introduction

Accurate terrain models are critical for 2D hydraulic habitat modeling. In void areas where lidar pulses could not penetrate, such as through dense vegetation, beneath bridge decks, or in areas with low water clarity, NV5 interpolated the lidar point data across the voids to produce a void-interpolated DEM. In some cases, the resulting interpolated surfaces contained artifacts that misrepresented the underlaying topography or bathymetry, potentially biasing model predictions of depth and velocity. To improve terrain model representation, especially in depth-limiting areas related to fish passage, CDFW conducted additional topographic surveys.

B.2 Methods

Base stations for RTK-GPS and total station surveys were set up over control points with known coordinates and elevations. During the ground survey, NV5 established three base station control points using 6-inch mag hub nails, two of which were used for CDFW data collection. Prior to the lidar ground survey, CDFW staff installed nine base station control points using #4 rebar driven flush to the ground (Figures B-1 and B-2). NV5 reoccupied each of the control points installed by CDFW and provided adjusted coordinates and elevations. Base station coordinates were referenced to California Coordinate System of 1983 (2011) Zone 2, epoch 2022.50, and elevations in the North American Vertical Datum of 1988. All units were in U.S. survey ft. CDFW also used a control point established by the Department of Water Resources near lower Middle Creek. Staff used RTK-GPS to collect survey points in open-channel void areas with adequate GPS reception using "Fixed only" survey mode, with the horizontal and vertical accuracy limits set to 0.05 ft.

To survey void areas where RTK-GPS reception was not available (e.g., under bridge decks and within dense vegetation), staff established temporary control points and used a total station to collect the survey points (Figure B-3). Temporary control points were established with the RTK-GPS in "Fixed only" survey mode for a continuous period of 10 minutes.

Figure B-1. Survey setup showing a tripod for an RTK-GPS base station positioned over a ground control point.

Figure B-2. Close-up view of a tripod for an RTK-GPS base station positioned over a ground control point.

Figure B-3. Total station survey setup near a lidar void under a bridge on Scotts Creek, October 2024. The total station is in the foreground, with an RTK-GPS rover (right) and stadia rod with total station prism reflector (left) in the background.

B.3 Analysis

There were several steps involved in generating the new interpolated surfaces under bridges and in each of the identified void areas (see Figure B-4 for an example). We first identified lidar voids that required additional surveying to improve the accuracy of the streambed representation in the DEM (Figure B-4, Panels A and B). Some voids were obvious, such as those beneath bridges or where there was unexpected variation in elevation along the longitudinal profile of the streambed. Other voids were detected by running exploratory simulations in the 2D models using NV5's void-interpolated DEM as the terrain surface input. Staff analyzed these preliminary model outputs to identify specific lidar void areas that either: 1) produced anomalies in the predicted water surface profile, or 2) occurred in shallow creek sections where CLH passage could be restricted in low-flow conditions. Using the same control point network established for the lidar data acquisition, CDFW collected topobathymetric points in and around the identified voids and imported them into ArcGIS software to create a new terrain surface (Figure B-4, Panel C). After importing the survey points, we generated a triangulated irregular network (TIN) surface for each void area using the Delaunay conforming triangulation method. Finally, each of the TIN

outputs were converted into a georeferenced raster surface (Figure B-4, Panel D), which was then overlaid upon the void-interpolated DEM that was produced by NV5.

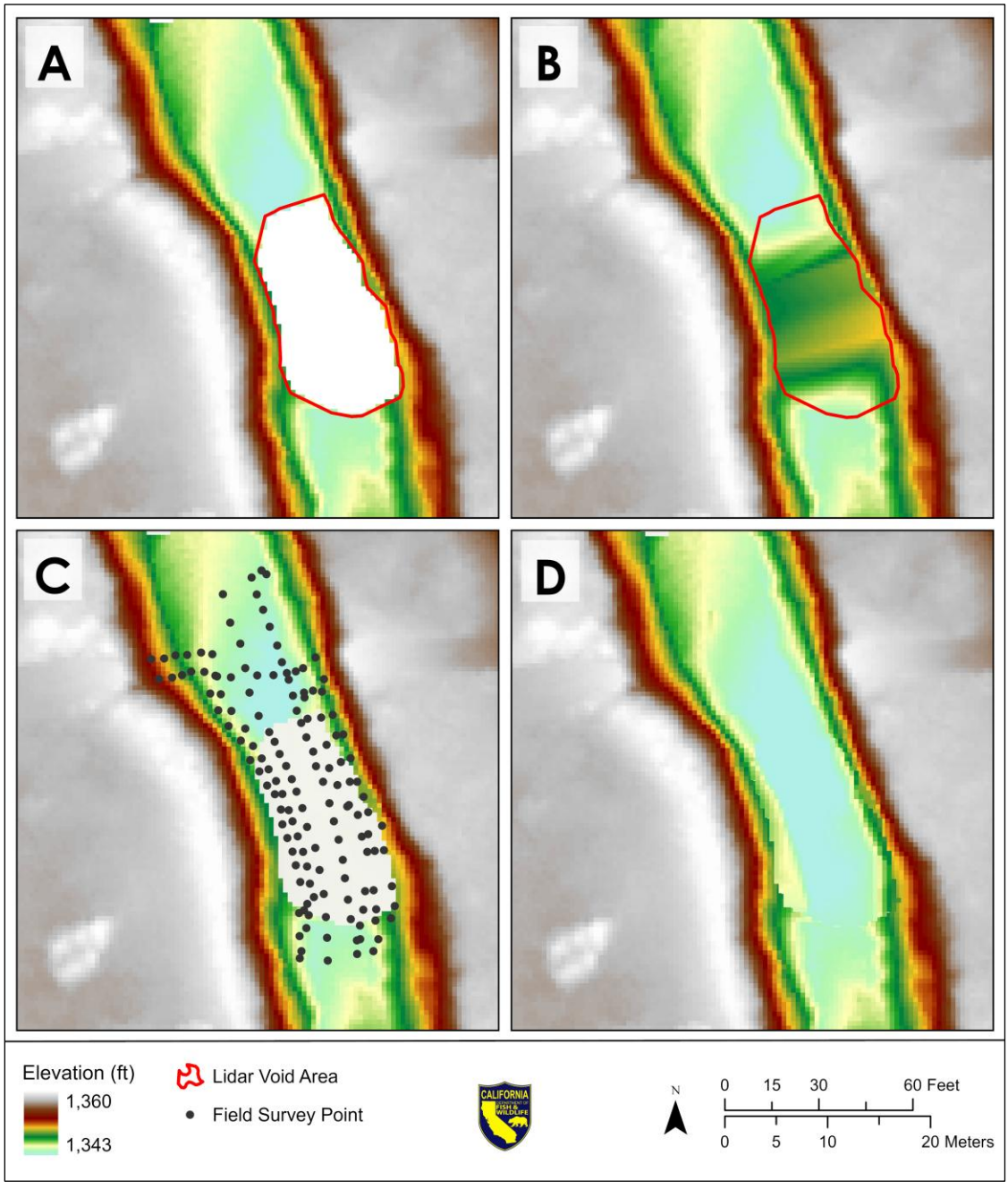

Figure B-4. Multi-panel map showing, A) a select void on Scotts Creek, B) the inaccurate representation of the terrain surface resulting from a bank-to-bank interpolation of the lidar data, C) CDFW collected survey points used to improve the terrain surface, and D) the updated interpolated surface from the survey points overlaid upon the NV5-generated DEM.

B.4 Results

In total, CDFW staff surveyed 71 voids (Figure B-5) under bridges and in select depth sensitive areas (DSAs) where the lidar-derived DEM did not accurately reflect the terrain surface. The points collected during these surveys were used to develop updated interpolated surfaces that could be combined with the void-interpolated DEM to make an updated terrain surface in the 2D HEC-RAS models.

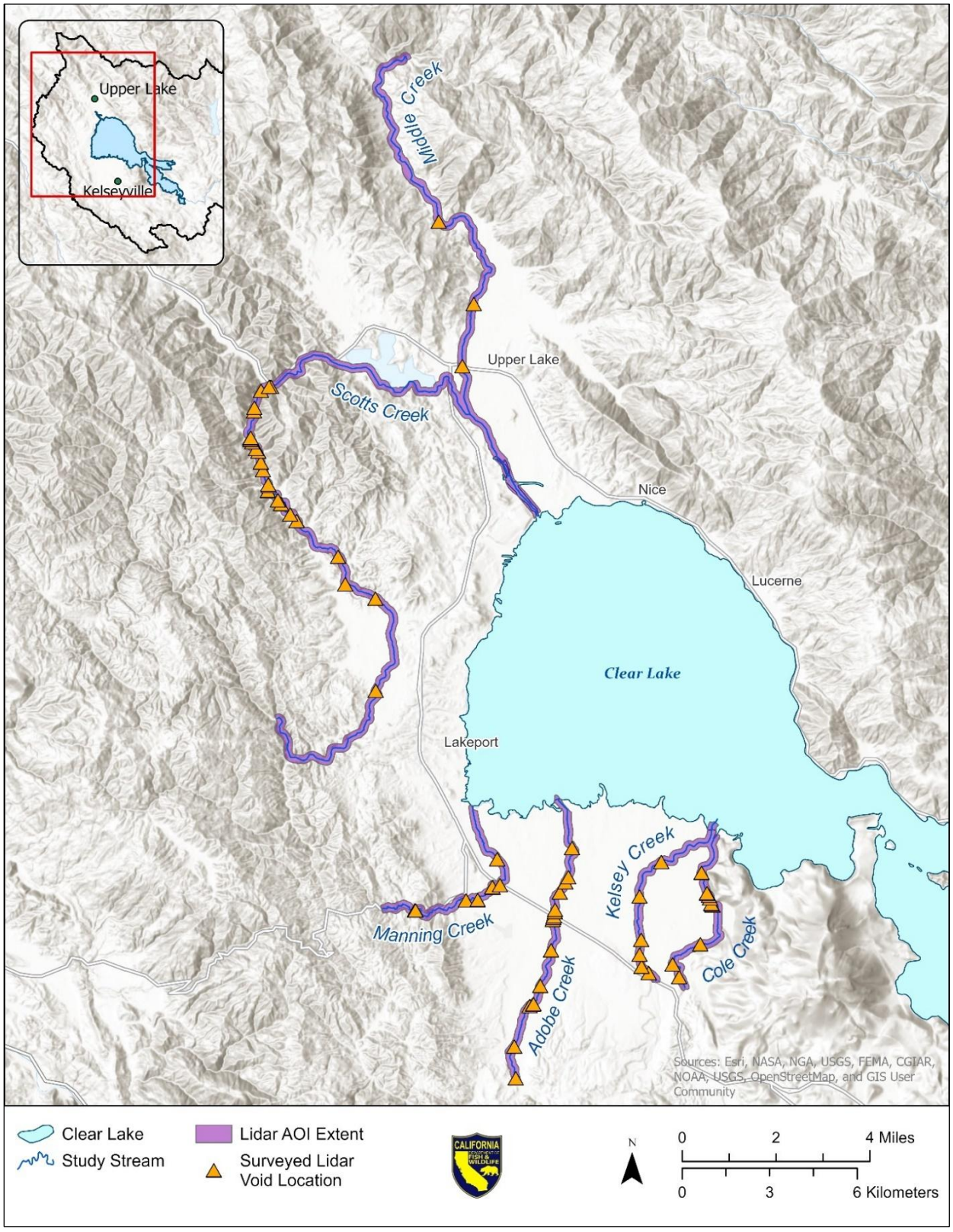

Figure B-5. Map of the lidar area of interest (purple) and CDFW-surveyed void areas (orange triangles) used to supplement the lidar data.

APPENDIX C: DISCHARGE AND WATER SURFACE ELEVATION MEASUREMENTS FOR 2D MODEL CALIBRATION

C.1 Introduction

CDFW collected field discharge measurements to generate predictive relationships between flow and water levels for each of the six study tributaries. Discharge, or flow, is the volume of water passing a certain point per unit of time. Water surface elevation (WSE) is comparable to water depth but specifically measures the height of the water column to a fixed vertical reference point, or datum. During spring of 2024, CDFW collected field discharge and WSE measurements along the longitudinal profile for each tributary length to calibrate the 2D hydraulic habitat models.

C.2 Methods

We measured discharge in each study tributary following CDFW Instream Flow Program's Standard Operating Procedure (SOP) for Discharge Measurements in Wadeable Streams in California (CDFW 2020). Field staff used a Hach FH950 velocity flow meter at locations with a reasonably straight flow path and with flow perpendicular to the cross sectional transect. Field staff selected transects in reaches with steady, uniform flow and were free of obstructions like large rocks or vegetation. Each transect was aligned perpendicular to the channel and wide enough to capture at least twenty sub-section flow measurements following the mid-section method. This method divides the stream's cross-sectional area into sub-sections where the width of each sub-section extends from the midpoint of the previous measurement location to the midpoint of the next measurement location. Staff determined sub-sectional discharge by multiplying sub-section width, depth, and velocity. The sum of each sub-section discharge results in total tributary discharge at a given site. Staff aimed for each sub-section to represent approximately 5 percent of the total discharge with a maximum of 10 percent allowed under the SOP. After a discharge measurement was complete, staff reviewed sub-section flow against total flow to determine if the measurement was reliable. All quality assurance followed the Instream Flow Program's Quality Assurance Plan (CDFW 2023).

To relate discharge to water depth, we collected WSE measurements at discharge sites and along the wetted edge of each study tributary's longitudinal profile using an RTK-GPS survey rover (Figures C-1 to C-6). These rovers were programmed to measure WSE data using a 30-second averaged collection period in "Fixed only" mode, meaning the location and elevation could only be recorded if the vertical and horizontal variance was within 0.05 ft. Staff collected

WSE measurements when the RTK-GPS had sufficient reception, typically when there was clear weather and limited vegetation cover.

Figure C-1. CDFW field staff measuring water surface elevation and discharge on Adobe Creek near Adobe Reservoir, April 2024.

Figure C-2. CDFW field staff measuring water surface elevation and discharge on Cole Creek near Soda Bay Road, April 2024.

Figure C-3. CDFW field staff measuring water surface elevation and discharge on Kelsey Creek near Finley East Road, April 2024.

Figure C-4. CDFW field staff measuring water surface elevation and discharge on Manning Creek near Soda Bay Road, April 2024.

Figure C-5. CDFW field staff measuring water surface elevation and discharge on Middle Creek near Elk Mountain Road, May 2024.

Figure C-6. CDFW field staff measuring water surface elevation and discharge on Scotts Creek near Cow Mountain Recreation Area, May 2024.

C.3 Results

A total of 46 discharge measurements and approximately 1,100 WSE measurements were collected from March to May 2024 (Table C-1 and Table C-2). Figures C-7 to C-11 illustrate where CDFW collected discharge and WSE data for each of the study tributaries that were within the lidar AOI (Appendix A).

Water surface elevation data were collected for each tributary across the following field discharge ranges in cubic feet per second (cfs): Cole Creek (3.5–17.8 cfs), Kelsey Creek (47.2–54.6 cfs), Adobe Creek (3.8–44.0 cfs), Manning Creek (<1–16.0 cfs), Scotts Creek (12.2–24.5 cfs), and the main stem of Middle Creek (21.6–48.0 cfs).

Table C-1. The total number of discharge measurements and the collection period for when CDFW collected the data for each of the six study tributaries.

Tributary Name	Total	Collection Period
Adobe Creek	5	4/9/2024–4/11/2024
Cole Creek	4	3/8/2024–5/7/2024
Kelsey Creek	10	4/22/2024–4/25/2025
Manning Creek	12	4/2/2024–4/29/2024
Middle Creek	7	5/8/2024–5/10/2024
Scotts Creek	7	5/13/2024–5/16/2024

Table C-2. The total number of water surface elevations and the collection period for when CDFW collected the data for each of the six study tributaries.

Tributary Name	Total	Collection Period
Adobe Creek	293	4/9/2024–4/11/2024
Cole Creek	119	4/8/2024–5/7/2024
Kelsey Creek	114	4/22/2024–4/24/2024
Manning Creek	176	4/2/2024–4/29/2024
Middle Creek	245	5/8/2024–5/10/2024
Scotts Creek	155	5/8/2024–5/16/2024

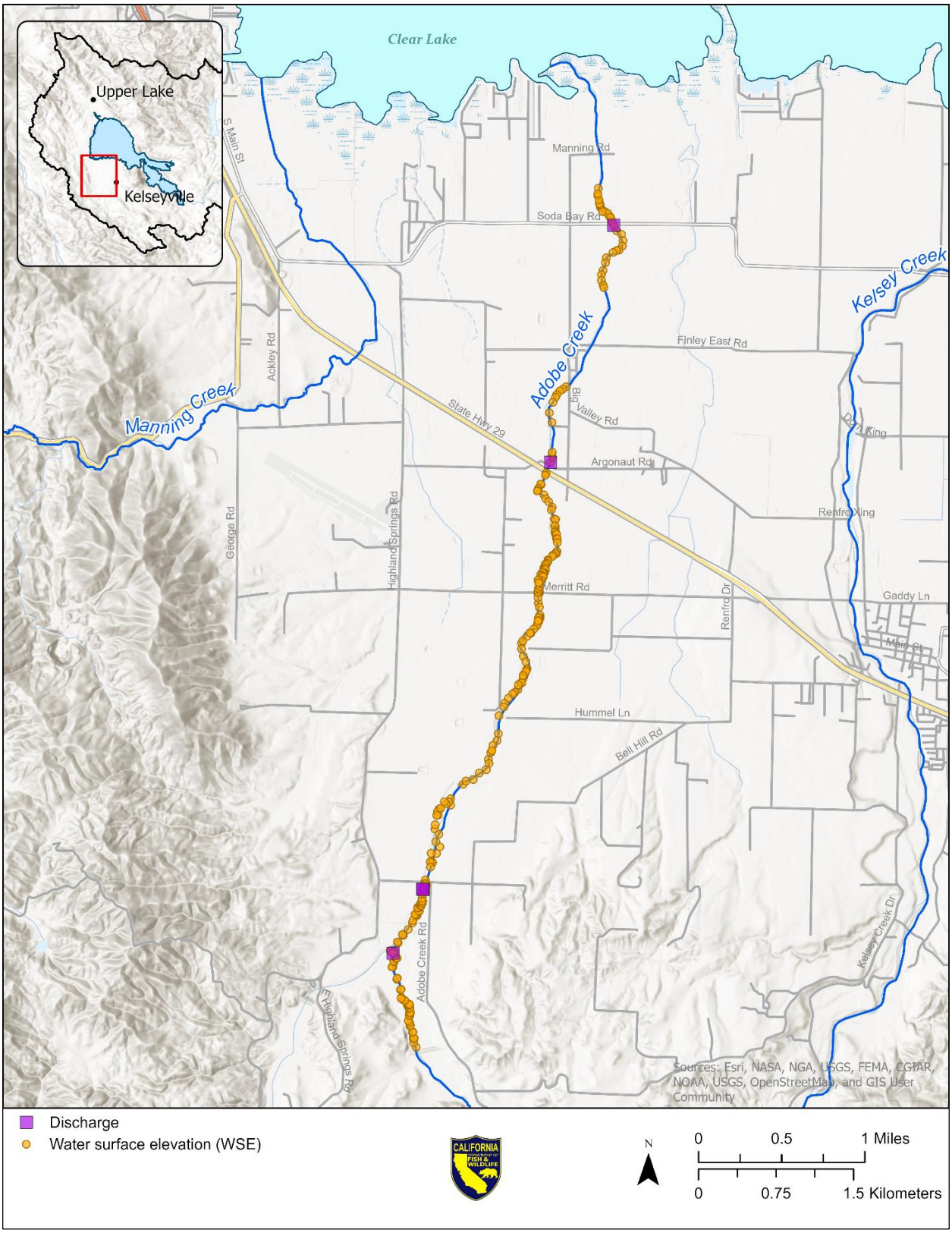

Figure C-7. Locations of water surface elevations (orange circles) and discharge measurements (purple squares) collected on Adobe Creek.

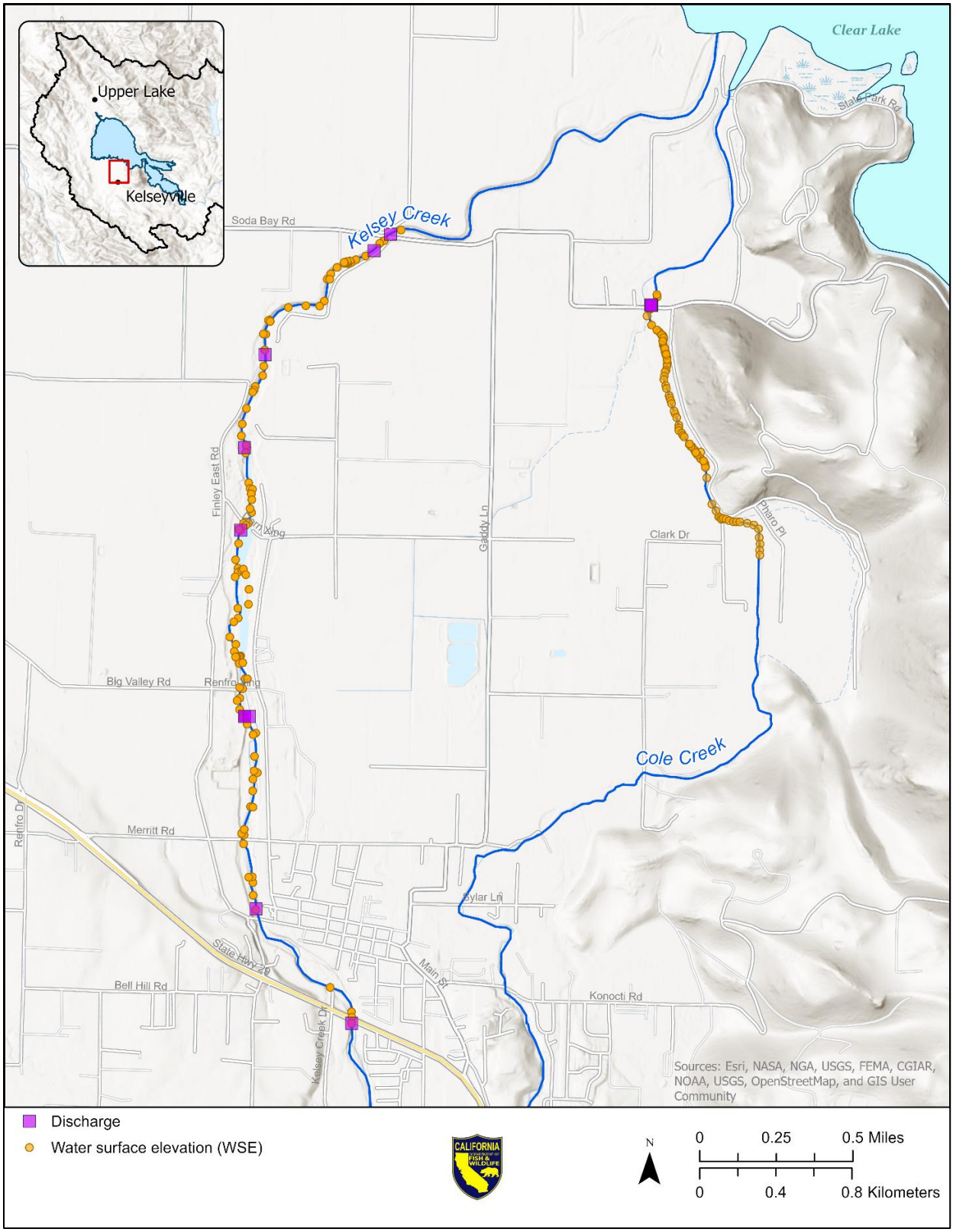

Figure C-8. Locations of water surface elevations (orange circles) and discharge measurements (purple squares) collected on Kelsey and Cole creeks.

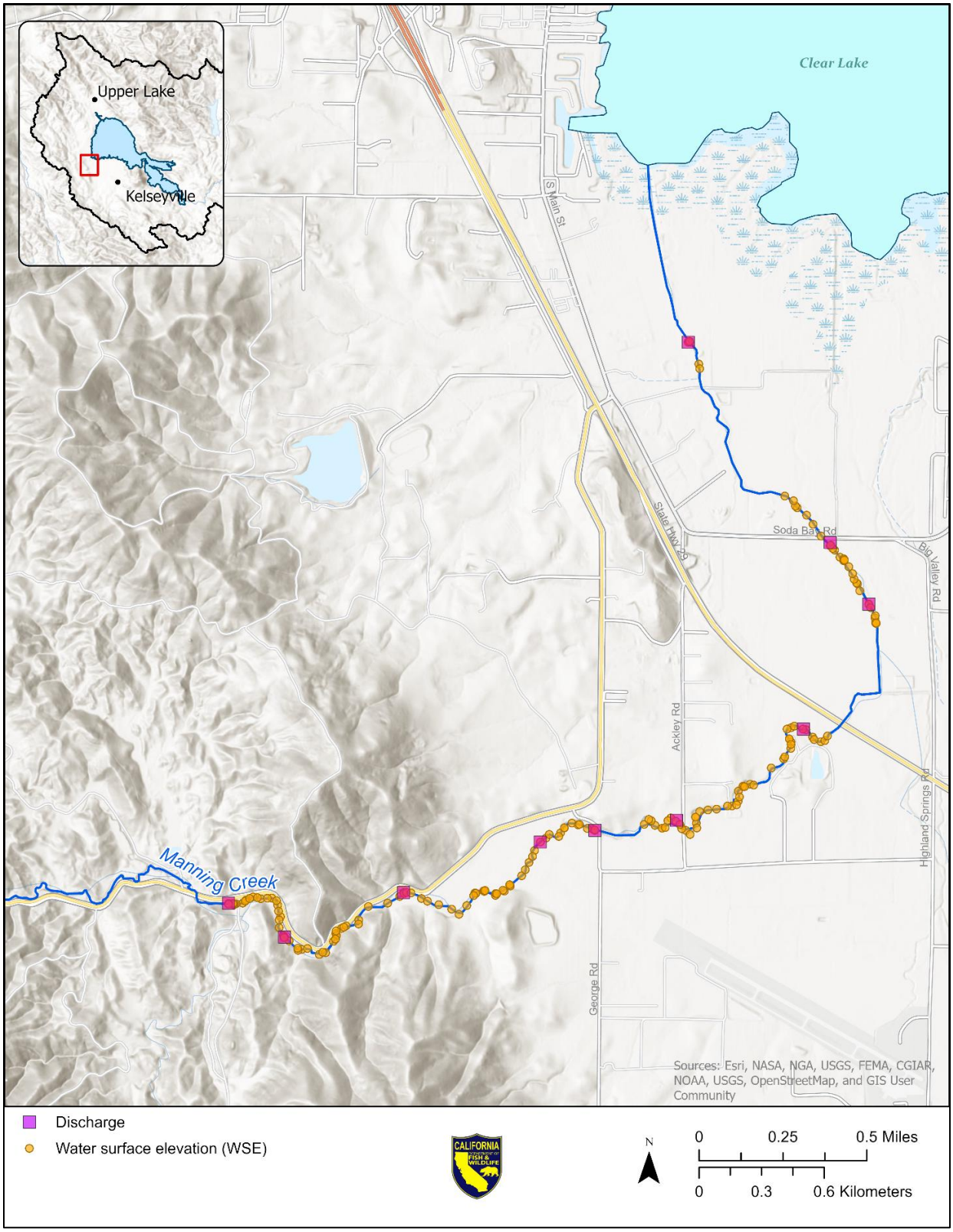

Figure C-9. Locations of water surface elevations (orange circles) and discharge measurements (purple squares) collected on Manning Creek.

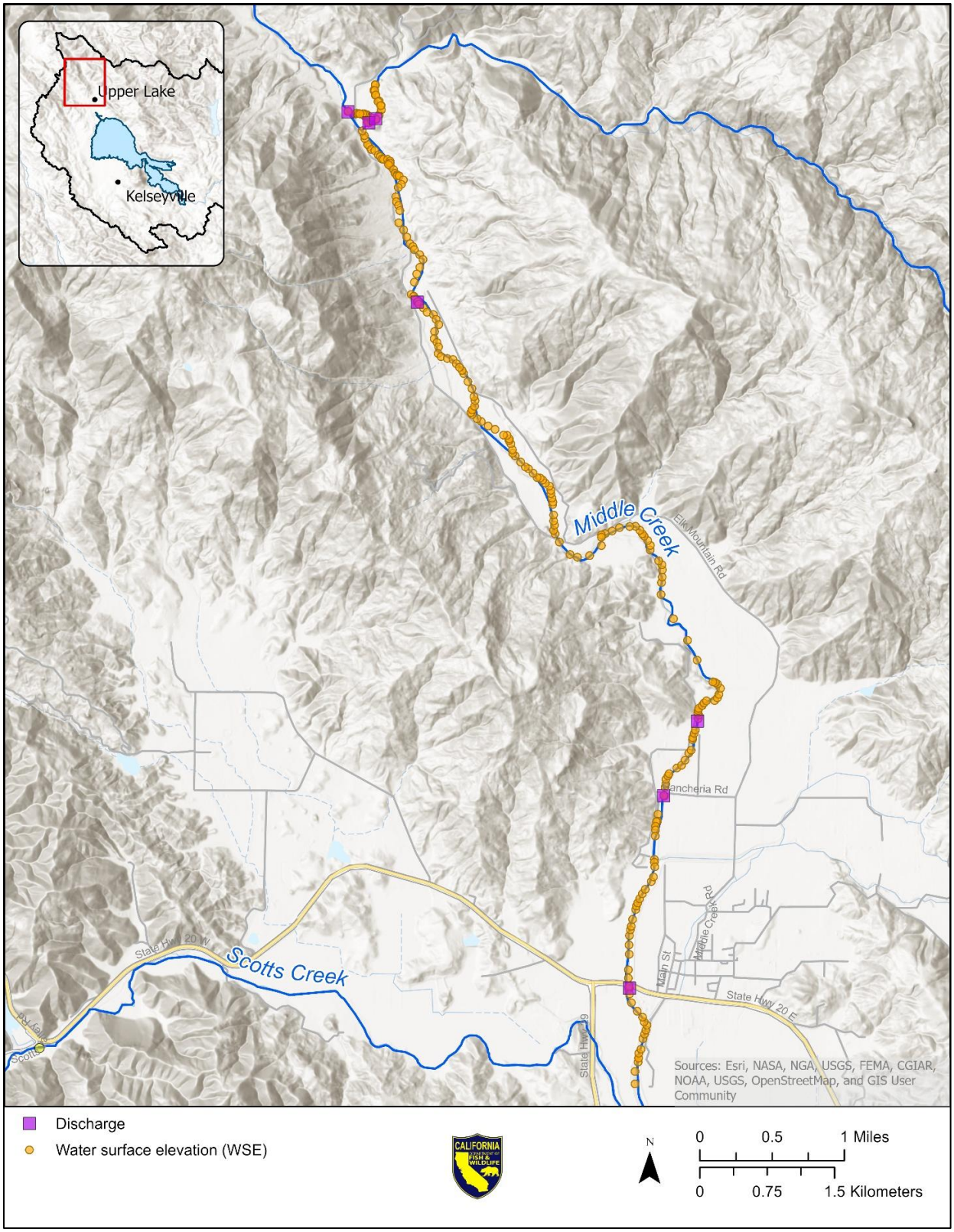

Figure C-10. Locations of water surface elevations (orange circles) and discharge measurements (purple squares) collected on Middle Creek.

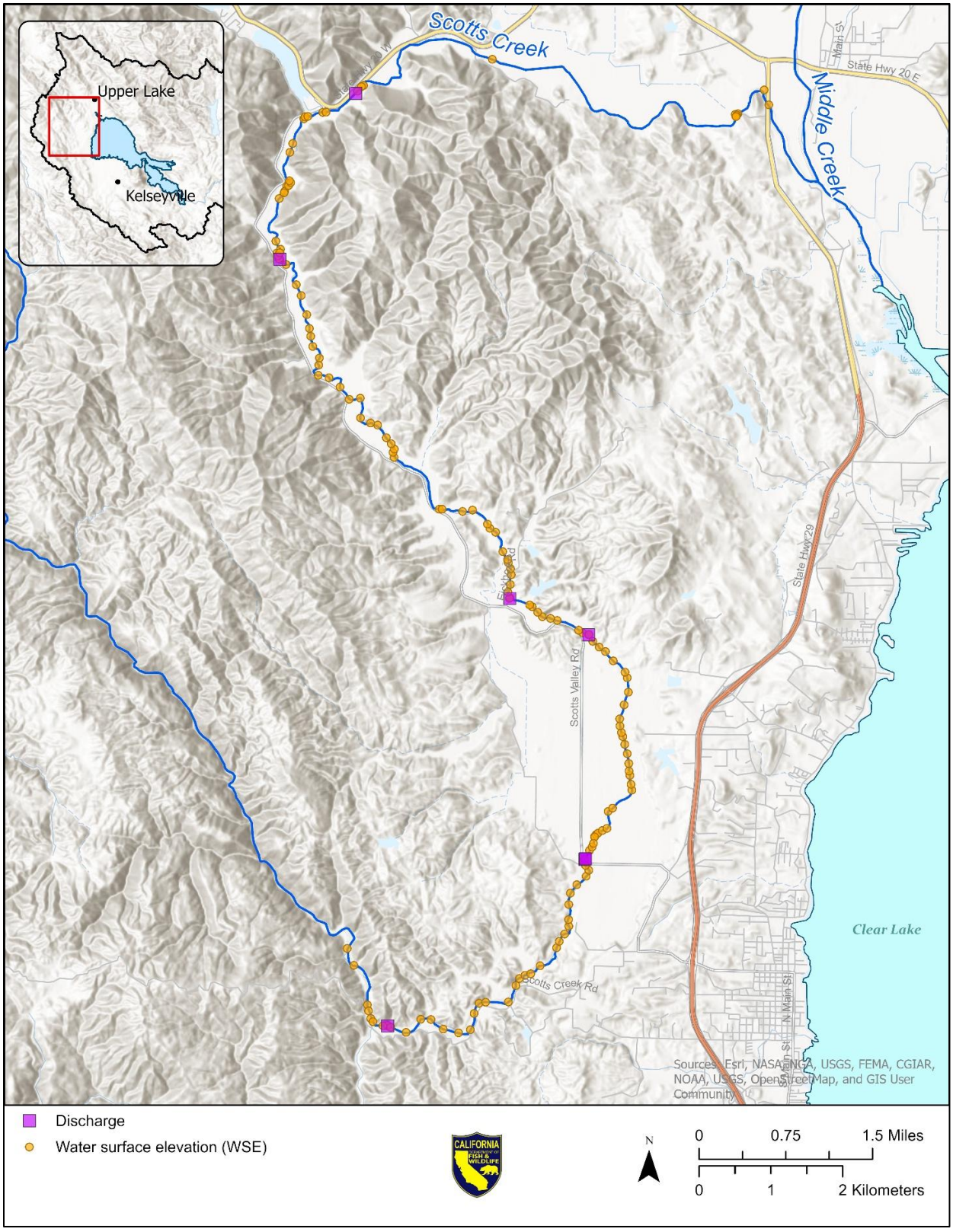

Figure C-11. Locations of water surface elevations (orange circles) and discharge measurements (purple squares) collected on Scotts Creek.

APPENDIX D: DEPTH AND VELOCITY MEASUREMENTS FOR 2D MODEL VALIDATION

D.1 Introduction

Hydraulic habitat model validation compares field measurements of depth and velocity with corresponding model-simulated values at known streamflows and locations. These comparisons provide a quantitative basis for evaluating how well the model reproduces real-world observations. Accurate representation between observed and predicted values demonstrates that the model can reliably simulate hydraulic conditions across a range of flows, supporting its application for CLH passage assessment.

D.2 Methods

Validation measurements consist of paired water depth and flow velocity measurements collected at a known location within a tributary. Depth and velocity are two primary hydraulic parameters used to specify criteria for flow-fish habitat relationships (Bovee 1982). CDFW collected validation data following U.S. Fish and Wildlife Service guidelines (USFWS 2011), focusing on precise, field-based data collection and rigorous statistical comparison with model predictions. All quality assurance followed Instream Flow Program's Quality Assurance Plan (CDFW 2023).

We measured water depth and velocity primarily near stream access points and in sections of each tributary where upstream and downstream movement was possible. Staff primarily collected measurements in wadable sections with discernible water flow. Each validation measurement consisted of a water depth and velocity reading using a HACH 950 flow meter, a top-setting rod, and an RTK-GPS unit to document its exact location. A minimum of 50 validation measurements were collected along each study tributary, as per (USFWS 2011) recommendations. Figures D-1 through D-6 show field staff collecting validation measurements in each study tributary, a process that typically requires a two-person team for efficiency.

Figure D-1. CDFW field staff measuring depth, velocity, and GPS coordinates on Adobe Creek near Adobe Reservoir, April 2024.

Figure D-2. CDFW field staff measuring depth, velocity, and GPS coordinates on Cole Creek near Clark Drive, April 2024.

Figure D-3. CDFW field staff measuring depth, velocity, and GPS coordinates on Kelsey Creek near Finley East Road, April 2024.

Figure D-4. CDFW field staff measuring depth, velocity, and GPS coordinates on Manning Creek near Highway 175, April 2024.

Figure D-5. CDFW field staff measuring depth, velocity, and GPS coordinates on Scotts Creek near Cow Mountain Recreation Area, May 2024.

Figure D-6. CDFW field staff measuring depth, velocity, and GPS coordinates on Middle Creek near the confluence with Scotts Creek, May 2024.

Prior to recording depth and velocity, we collected discharge measurements to later verify that modeled flow conditions matched with field conditions (Appendix C, Appendix G). We then used the measured field discharge to run a 2D hydraulic model simulation for the corresponding flow. Field depth and velocity measurements were compared to the modeled values at matching locations and flow conditions. During field collection, crews recorded GPS coordinates, water depth, and water velocity on standardized field forms. Each measurement point received a unique identifier that linked the location, depth, velocity, and associated metadata, including date, start and end times, staff names, tributary, access point, photo numbers, and equipment used. Staff reviewed field forms for accuracy and completeness. Location measurements were collected using the same RTK-GPS survey methods described in Appendix B.

D.3 Results

CDFW collected over 500 paired depth and velocity measurements during April and May of 2024 (Table D-1). Figures D-7 through D-12 show the locations of water depth and velocity measurements along each tributary along with field discharge measurement locations. Validation data were collected within the model boundaries established by lidar coverage (Appendix A), focusing on wadable tributary reaches where flow could be measured and RTK-GPS signal was reliable.

Figure D-13 and Figure D-14 show the range of field water depths and velocity measurements collected concurrently with calibration discharge measurements (Appendix C). Depths were comparable among the six tributaries, with median depths falling between 0.5 ft and 1.0 ft across all tributaries. Average velocities showed greater variability between tributaries, with median values ranging from approximately 0.8 ft/s (Manning Creek) to 1.6 ft/s (Kelsey Creek). These measurements collectively characterize the range of hydraulic conditions potentially available for CLH passage across the study tributaries during spring recession flows.

Table D-1. Summary of depth and velocity measurement totals and collection periods for the six study tributaries.

Tributary Name	Total	Collection Period
Adobe Creek	70	4/9/2024–4/11/2024
Cole Creek	53	4/8/2024–5/7/2024
Kelsey Creek	111	4/22/2024–4/24/2024
Manning Creek	83	4/2/2024–4/29/2024
Middle Creek	146	5/8/2024–5/10/2024
Scotts Creek	121	5/13/2024–5/15/2024

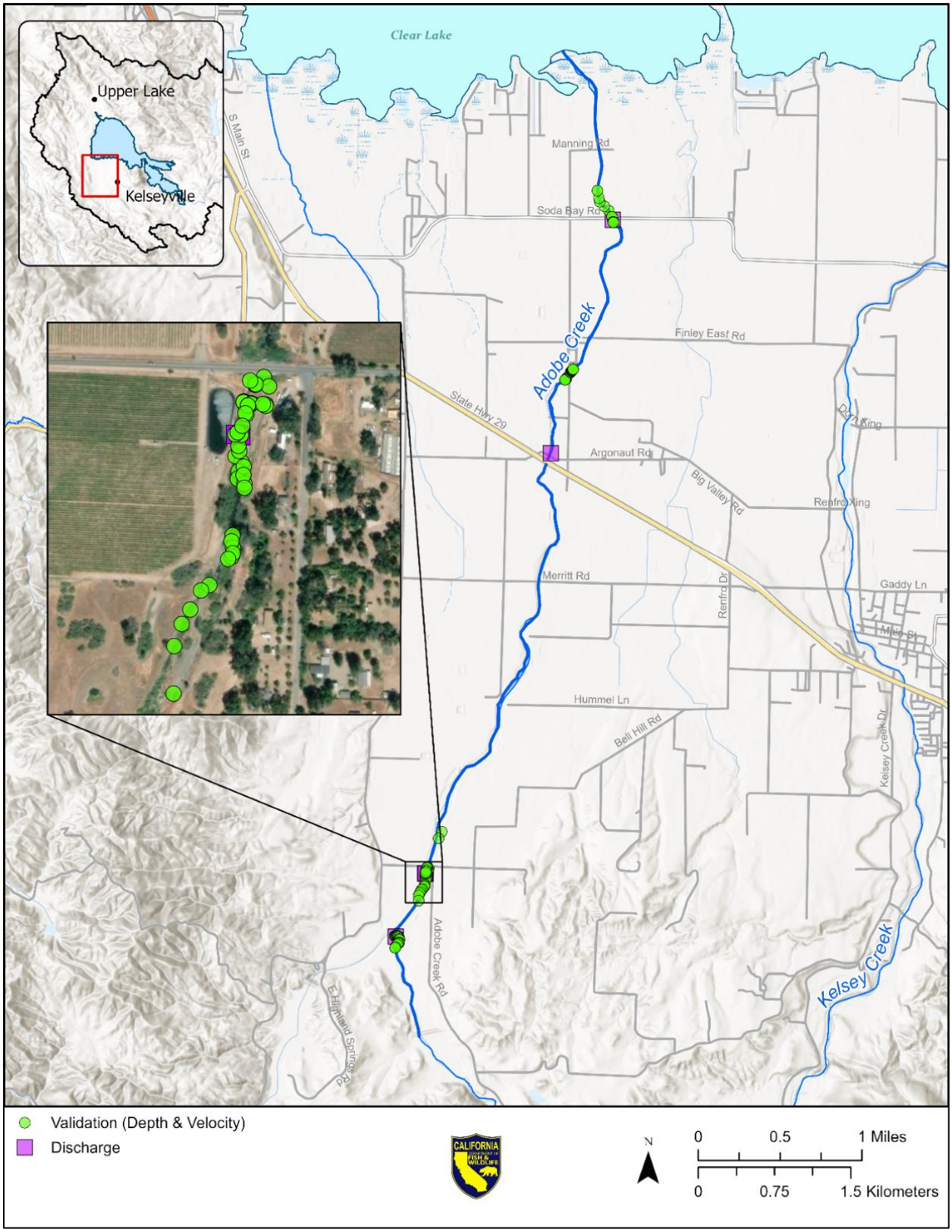

Figure D-7. Locations of validation data (depth and velocity, green points) and discharge measurements (purple squares) on Adobe Creek.

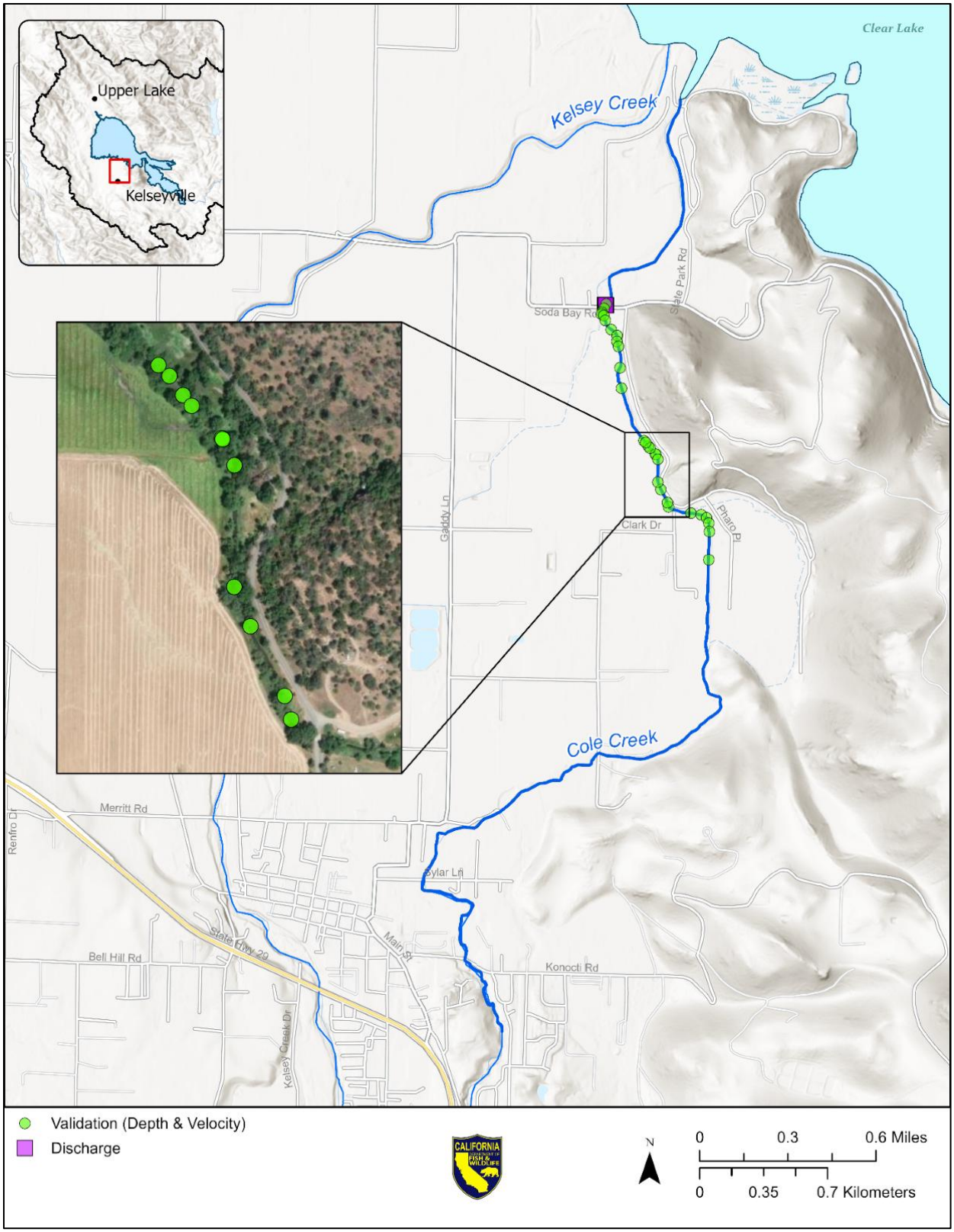

Figure D-8. Locations of validation data (depth and velocity, green points) and discharge measurements (purple squares) on Cole Creek.

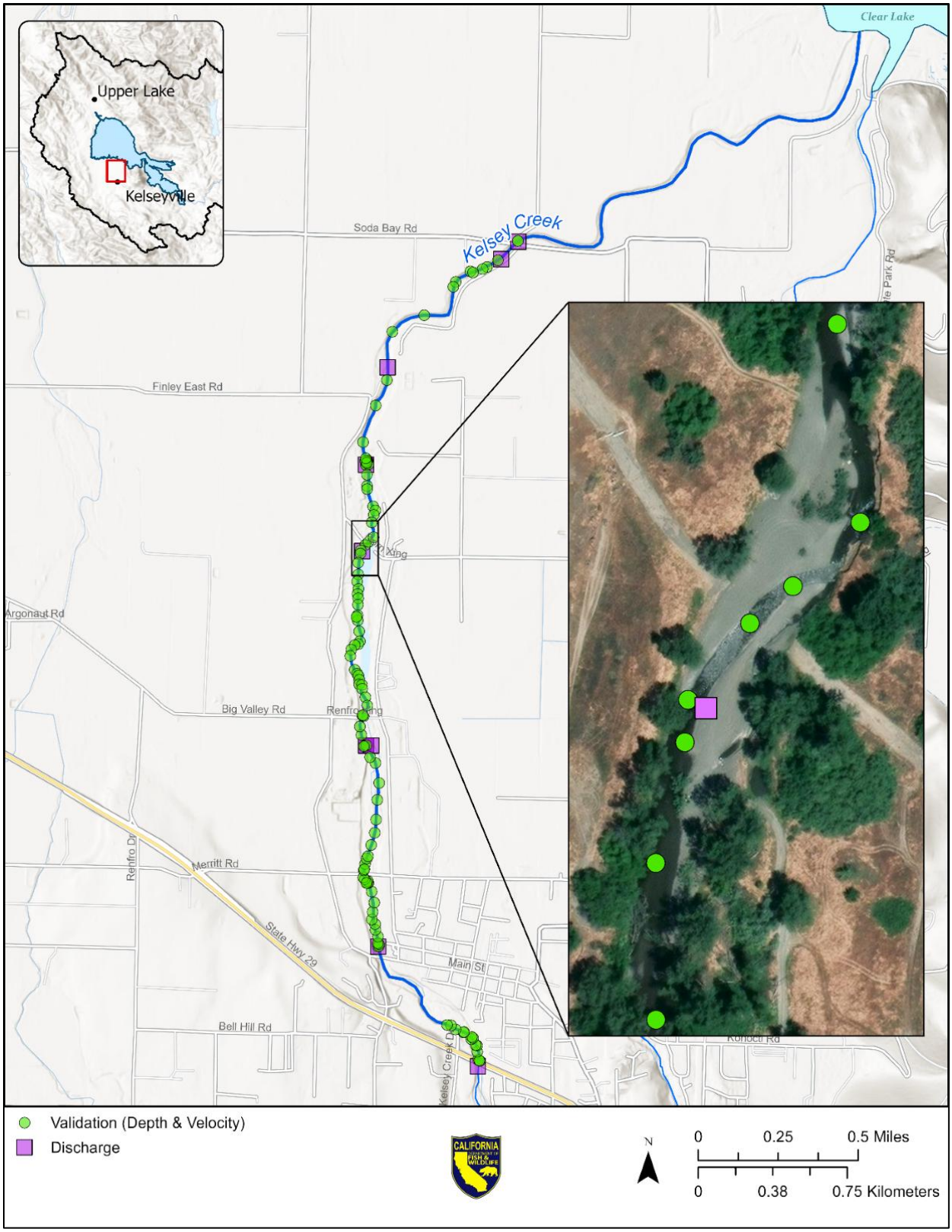

Figure D-9. Locations of validation data (depth and velocity, green points) and discharge measurements (purple squares) on Kelsey Creek.

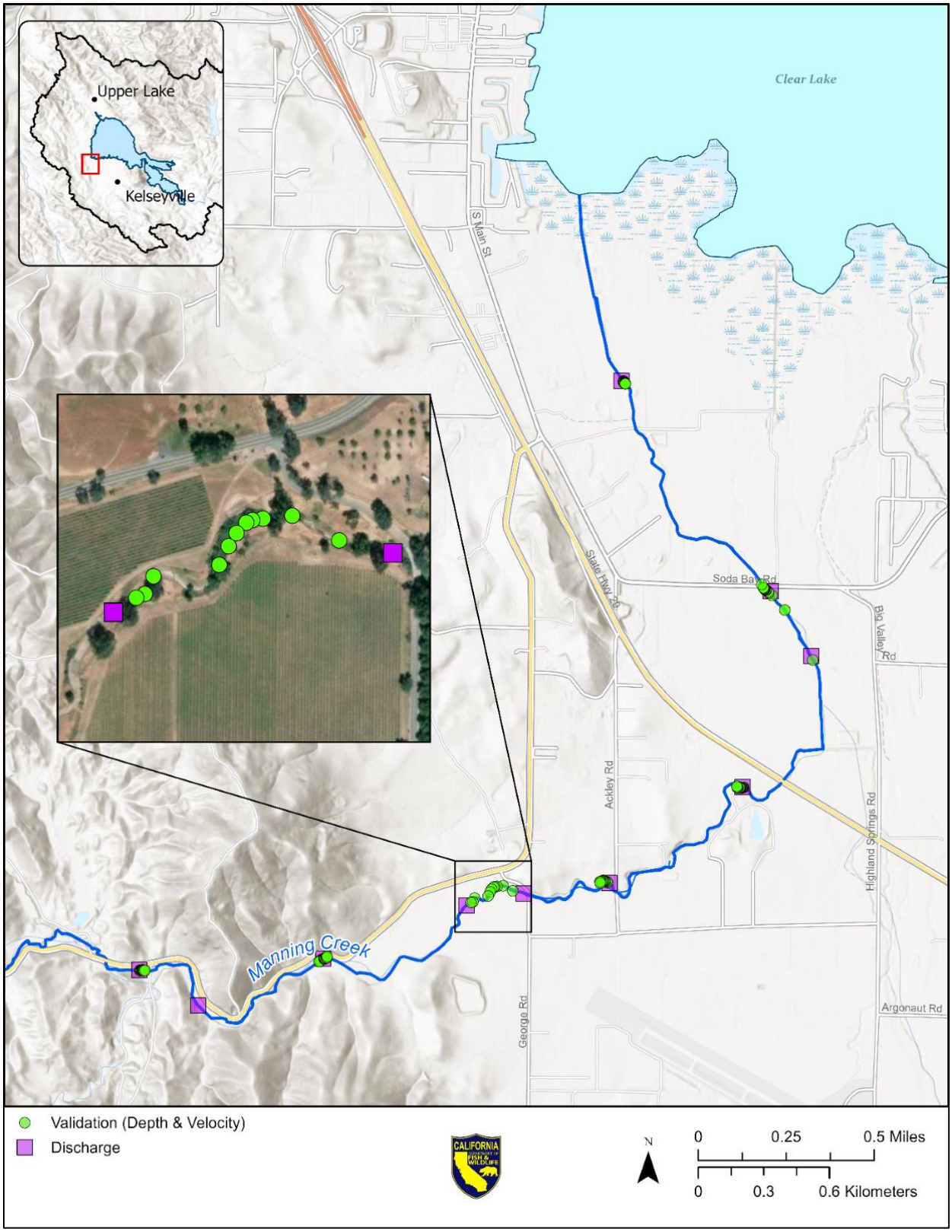

Figure D-10. Locations of validation data (depth and velocity, green points) and discharge measurements (purple squares) on Manning Creek.

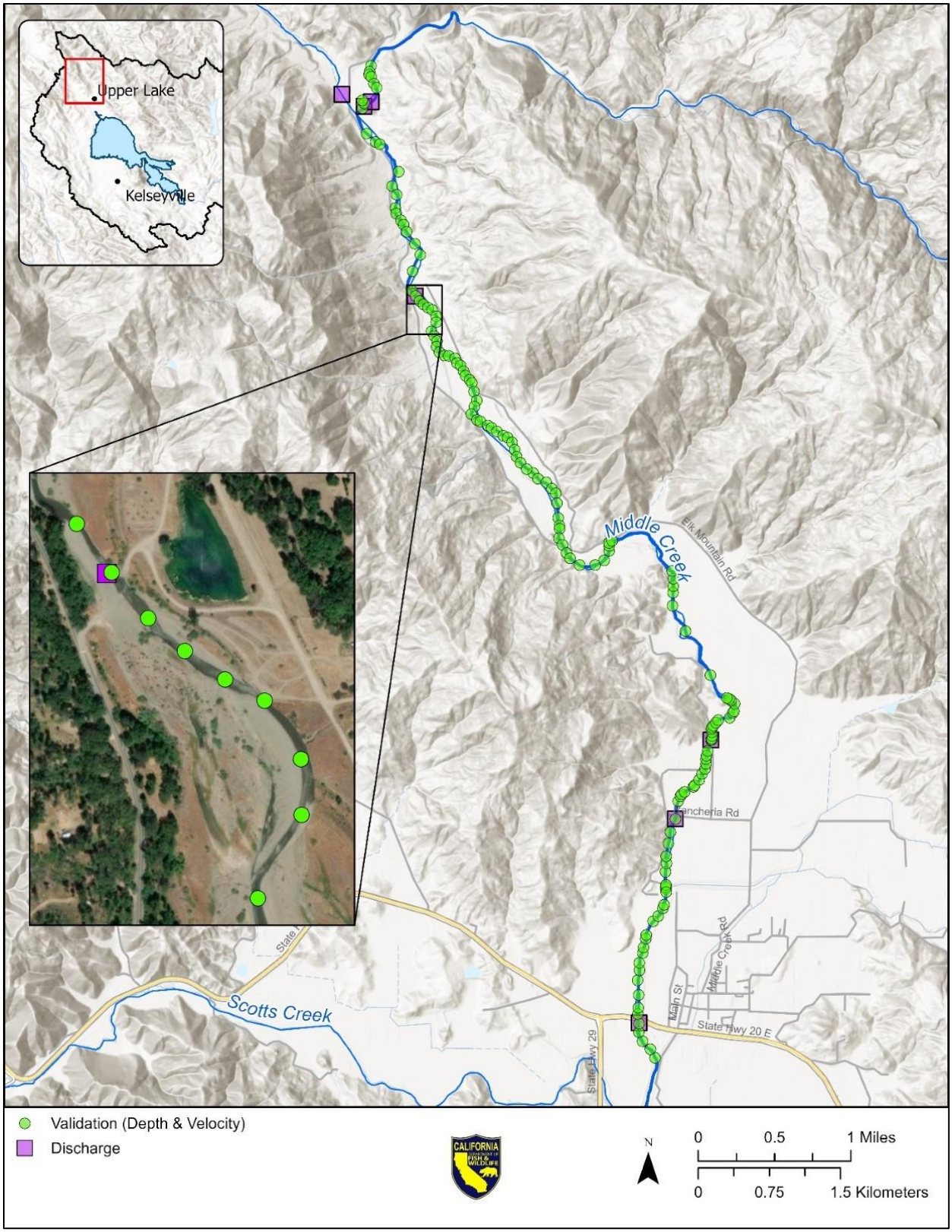

Figure D-11. Locations of validation data (depth and velocity, green points) and discharge measurements (purple squares) on Middle Creek.

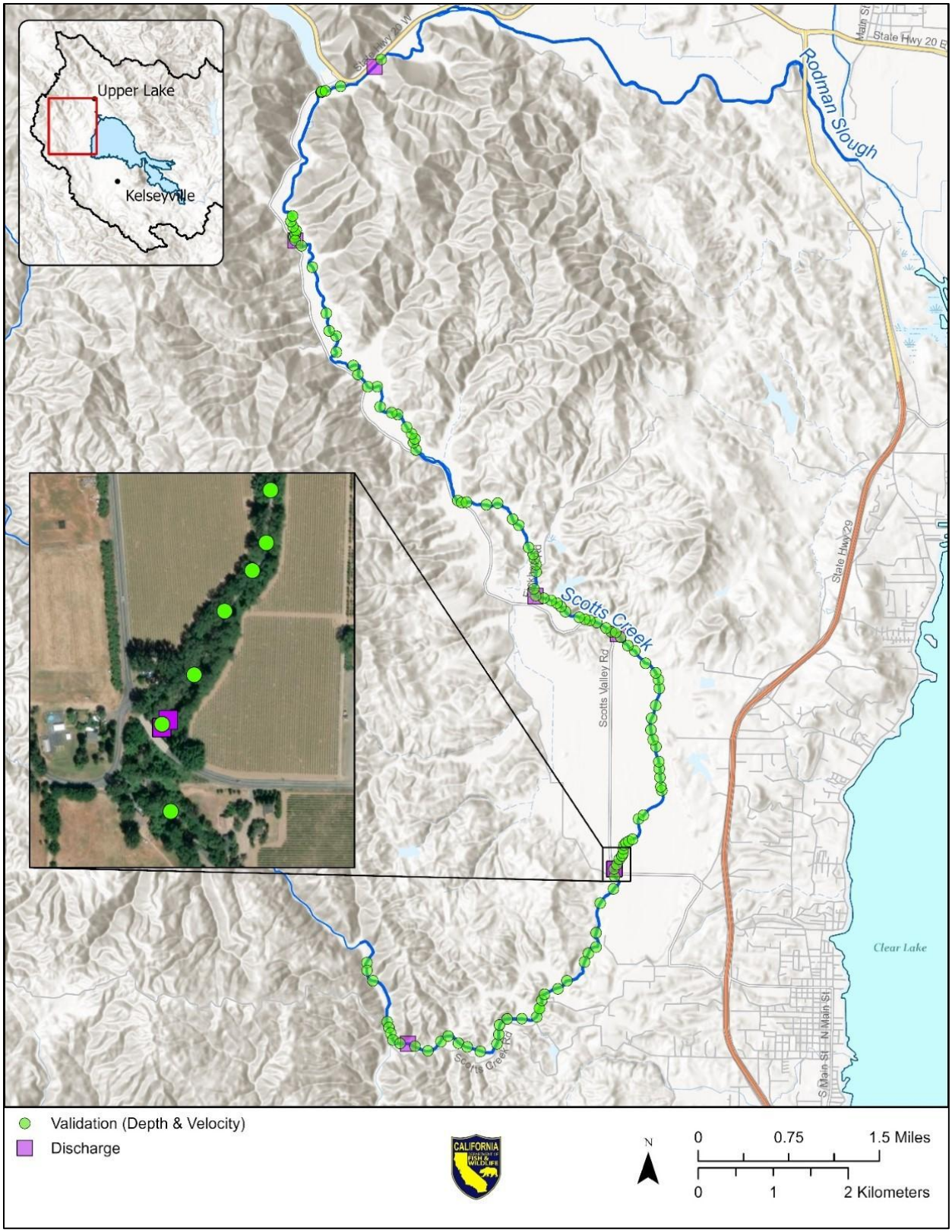

Figure D-12. Locations of validation data (depth and velocity, green points) and discharge measurements (purple squares) on Scotts Creek.

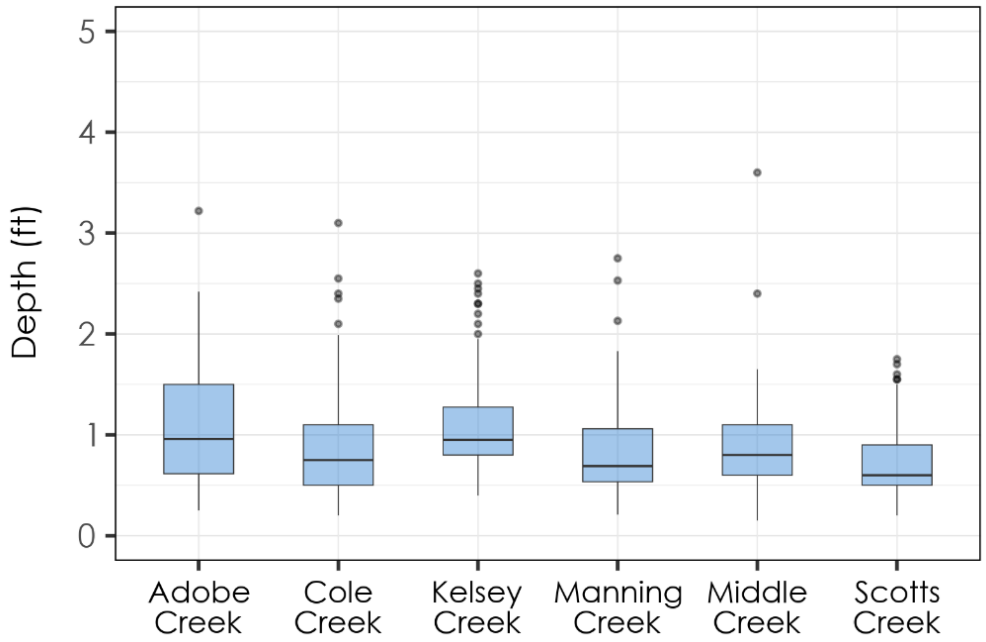

Figure D-13. Distribution of field-measured water depths across the six study tributaries used for 2D model validation. Bars show the interquartile range (25th–75th percentile), whiskers extend 1.5x the interquartile range, horizontal lines mark medians, and outliers appear as points.

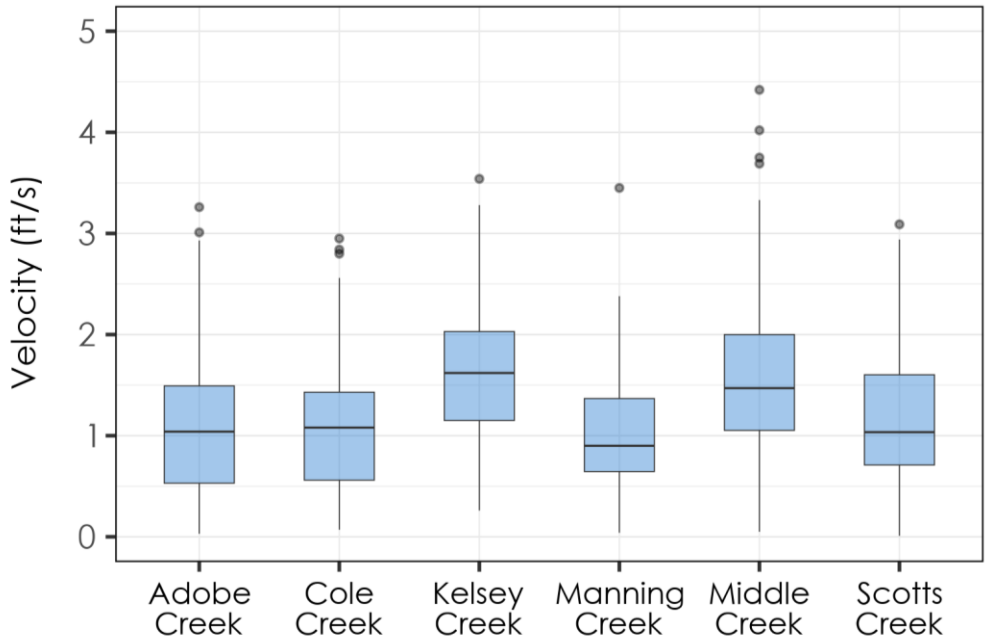

Figure D-14. Distribution of field-measured velocity across the six study tributaries used for 2D model validation. Bars show the interquartile range (25th–75th percentile), whiskers extend 1.5x the interquartile range, horizontal lines mark medians, and outliers appear as points.

APPENDIX E: PEBBLE COUNTS TO ESTIMATE INITIAL CHANNEL ROUGHNESS

E.1 Introduction

CDFW used pebble count data to estimate initial channel roughness for each of the six tributaries. We conducted pebble count surveys along the longitudinal profile of each tributary to complement the WSE data collected for 2D model calibration (Appendix C). Represented as a dimensionless coefficient, the Manning's *n* values derived from the pebble counts provided the initial estimates of streambed roughness used in model calibration (Appendix G).

The 2D models were calibrated by adjusting channel roughness until the simulated WSE slope matched the longitudinal water surface profile points collected in the field. The HEC-RAS module used Manning's *n* to estimate channel roughness, which accounts for: 1) surface roughness, 2) vegetation, 3) channel irregularity, 4) channel alignment, 5) silting and scouring, 6) in-channel obstructions, 7) channel size and shape, 8) stage and discharge, 9) seasonal changes, and 10) suspended material and bed load (Chow 1959). The 2D models account for channel irregularity, channel alignment, in-channel obstructions and channel size and shape through the underlying terrain. Thus, for 2D models, channel roughness primarily consists of surface roughness and vegetation.

Cowan (1956) calculated Manning's *n* coefficient by:

$$n = (n_0 + n_1 + n_2 + n_3 + n_4) m_5$$

Where n_0 represents a basic value for a straight, smoothly uniform channel placed in the natural channel bed materials, n_1 accounts for irregularities in the bed surface, n_2 accounts for the shape and relative size of the channel cross-section, and n_3 accounts for instream obstructions if present, and n_4 accounts for instream vegetation if present. The factor m_5 then accounts for the meandering of the channel. The roughness components n_1, n_2, n_3, and m_5 are accounted for in the 2D model by level of complexity of the digital terrain model developed from the lidar and topographic surveying (Appendices A and B). The term n_0 can be estimated by determining the particle size distribution of the stream bed. CDFW applied the Wolman pebble count procedure (Wolman 1954) to estimate particles size distributions at sampling sites along the longitudinal profile of each tributary. We then computed Manning's *n* values from these distributions using the relationships developed by Bray (1979). The resulting Manning's *n* values provided the initial estimate of channel roughness for each tributary 2D model.

E.2 Methods

CDFW selected pebble count sites near surveyed structures and DSAs to ensure representative substrate conditions and reasonable field access. Pebble count transects were oriented diagonally across the channel and extended between bankfull edges. At each transect turn, field staff recorded RTK-GPS point locations along the bankfull edge to document where sampling took place (Figure E-1). Pebbles, or particles, were randomly selected using the step-toe procedure and categorized into pre-defined size bins (WVDEP 2025). CDFW measured the intermediate diameter of each pebble in millimeters (mm) with a gravelometer (Figure E-2), sampling at least 100 pebbles per site (Wolman 1954). Verified pebble count data were entered into Microsoft Excel spreadsheets for each site and later compiled in the software R to generate a single dataset for visualization and for calculating the median (D_{50}) particle size. To calculate D_{50} values, we numerically ordered the pebble count data by size, tallied the frequency of each bin size, and computed cumulative distribution. The particle size at 50% of the distribution defined the median particle size (D_{50}).

We used Equation 1 (Bray 1979) to determine the preliminary Manning's *n* at a series of sampled sites (Table E-1) within each tributary as follows:

$$n = 0.0593\, {D_{50}}^{0.179} \qquad \text{(Equation 1)}$$

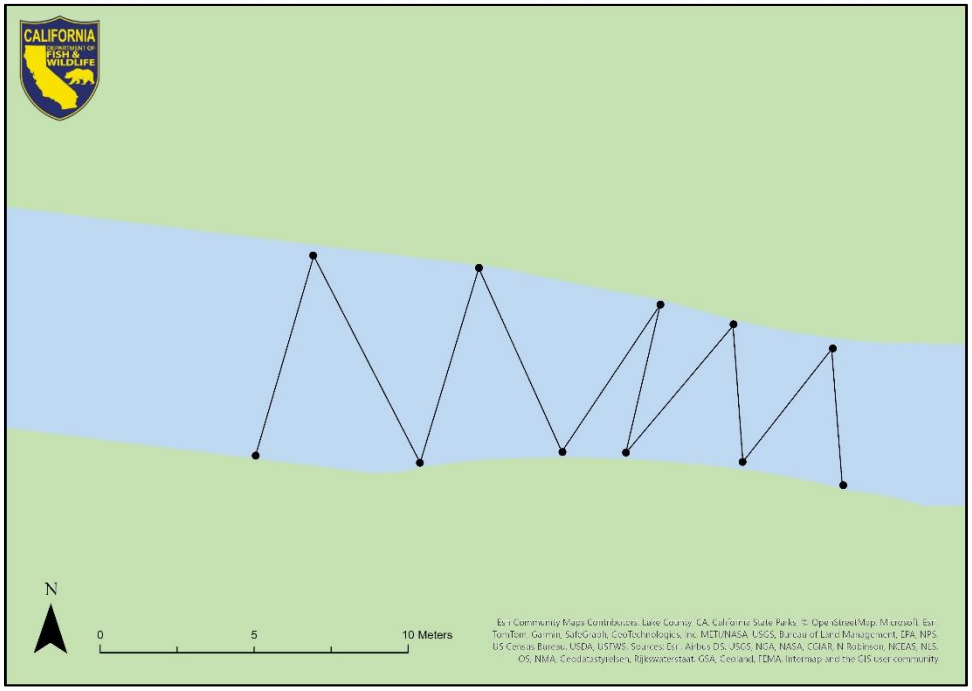

Figure E-1. Example of pebble count RTK-GPS points at bankfull edge on Manning Creek upstream of George Road Bridge.

Figure E-2. Image of gravelometer used to conduct pebble count surveys. Numbers adjacent to each square opening indicate the particle size class (in mm) for that bin.

E.3 Results

We completed pebble count surveys at 36 sites. Across all sites, D_{50} values were generally less than 52 mm, the approximate size of a bottle cap (Figures E-4 through E-9). The highest D_{50} (51 mm) occurred at Adobe Creek near Highway 29, while the lowest values (2 mm) were measured in Manning Creek near the Land Trust and lower Cole Creek locations (Figure E-3). Most D_{50} values (88% of all samples) ranged from 7.5 mm to 30 mm, corresponding to five bin sizes (8, 11 ,16, 22.6, and 32 mm). Particle size distribution in Adobe and Middle creeks showed the greatest variability across reaches (Figures E-4 and E-8). In Adobe Creek, D_{50} ranged from 14.8 mm to 51 mm, while in Middle Creek, D_{50} ranged from 7.9 mm to 45.5 mm.

Table E-1. Pebble count results for D_{50} at each study site with Manning's *n* values computed using Equation 1 (Bray 1979).

Tributary Name	Nearest Landmark	D_{50}	Manning's *n*
Adobe Creek	Argonaut Road	25.5	0.031
Adobe Creek	Downstream Bell Hill Road	16.9	0.029
Adobe Creek	Upstream Bell Hill Road	26.2	0.031
Adobe Creek	Big Valley Road	20.5	0.030
Adobe Creek	Finely East Road	18.0	0.029
Adobe Creek	Highland Springs	19.0	0.029
Adobe Creek	Highway 29	51.0	0.035
Adobe Creek	Merritt Road	14.8	0.028
Adobe Creek	Soda Bay Road	18.2	0.029
Cole Creek	Pharo Place	2.0	0.019
Cole Creek	Soda Bay Road	2.0	0.019
Cole Creek	Sylar Lane	24.4	0.031
Cole Creek	Clark Drive	22.6	0.030
Cole Creek	Konocti Road	21.5	0.030
Kelsey Creek	Upstream Detention Structure Road	26.2	0.031
Kelsey Creek	Upstream Detention Structure Road	12.3	0.027
Kelsey Creek	Dorn Crossing	14.3	0.028
Kelsey Creek	Merritt Road	21.4	0.030
Kelsey Creek	Soda Bay Road	15.8	0.028
Manning Creek	Near Granite Construction	11.8	0.027
Manning Creek	Upstream Highway 175 West	15.0	0.028
Manning Creek	Downstream Highway 175 West	11.6	0.027
Manning Creek	George Road	14.5	0.028
Manning Creek	Ackley Road	11.2	0.027
Manning Creek	Arizona Crossing	13.0	0.027
Manning Creek	Soda Bay Road	9.4	0.026
Manning Creek	Land Trust	2.0	0.019
Middle Creek	Upstream Highway 20	23.2	0.030
Middle Creek	Lower Seasonal Crossing	24.0	0.030
Middle Creek	Rancheria Road near Elk Mountain	19.0	0.029
Middle Creek	Rancheria Road Bridge	7.9	0.025
Middle Creek	Upper Seasonal Crossing	45.5	0.034
Middle Creek	West Fork Confluence	13.8	0.028
Scotts Creek	County Bypass	15.0	0.028
Scotts Creek	Cow Mountain	25.0	0.031
Scotts Creek	Eickhoff Road	7.5	0.025
Scotts Creek	Glen Eden Trail	19.0	0.029
Scotts Creek	Hendricks Bridge	30.0	0.032
Scotts Creek	Steep Access	11.7	0.027

Tributary Name	Nearest Landmark	D_{50}	Manning's *n*
Scotts Creek	Unnamed Road	16.5	0.028

Figure E-3. Sandy creek bed on Cole Creek at Soda Bay Road looking downstream (left) and upstream (right).

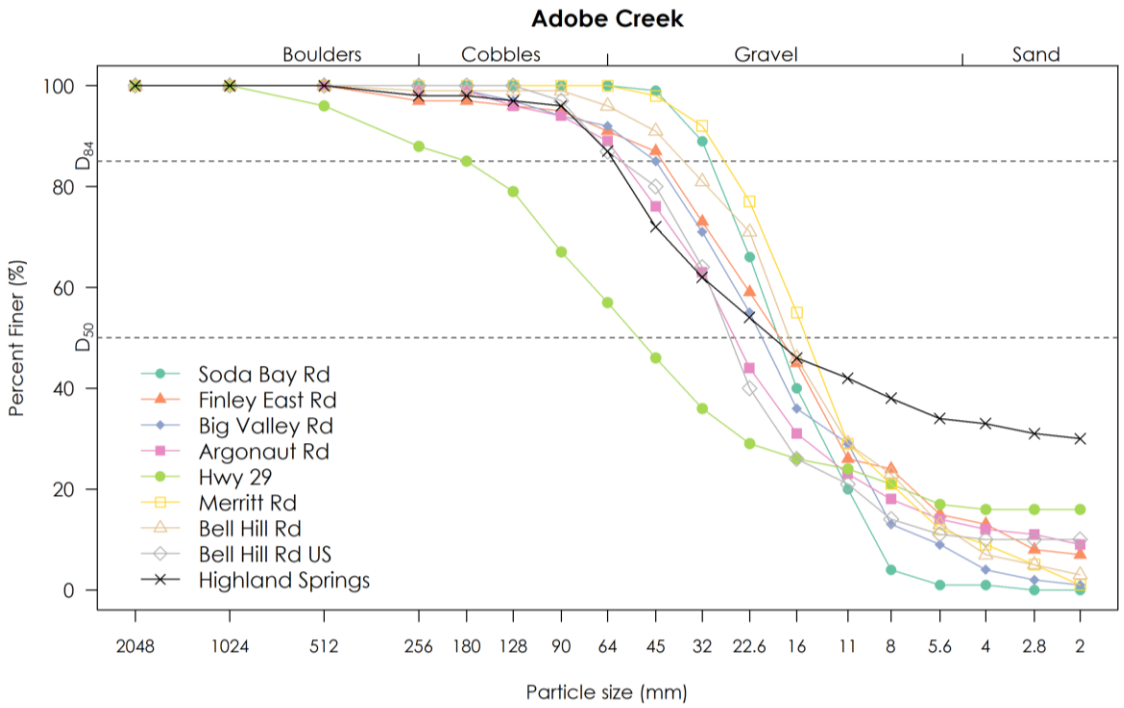

Figure E-4. Particle size distribution in Adobe Creek with sites ordered downstream to upstream.

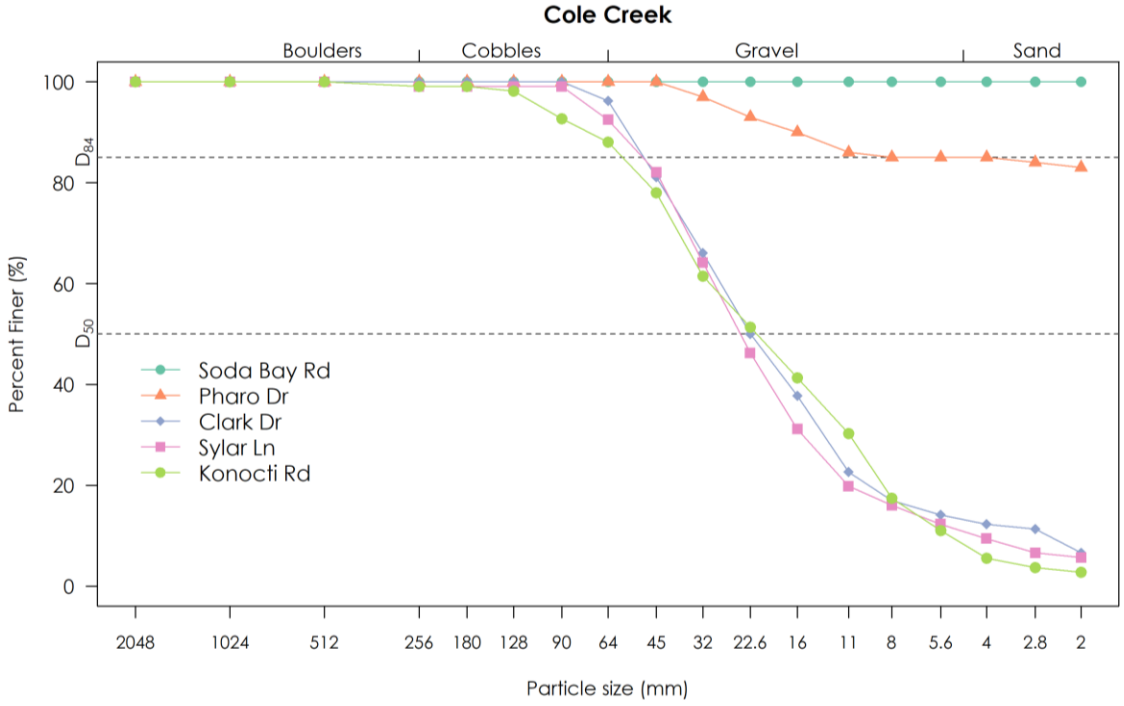

Figure E-5. Particle size distribution in Cole Creek with sites ordered downstream to upstream.

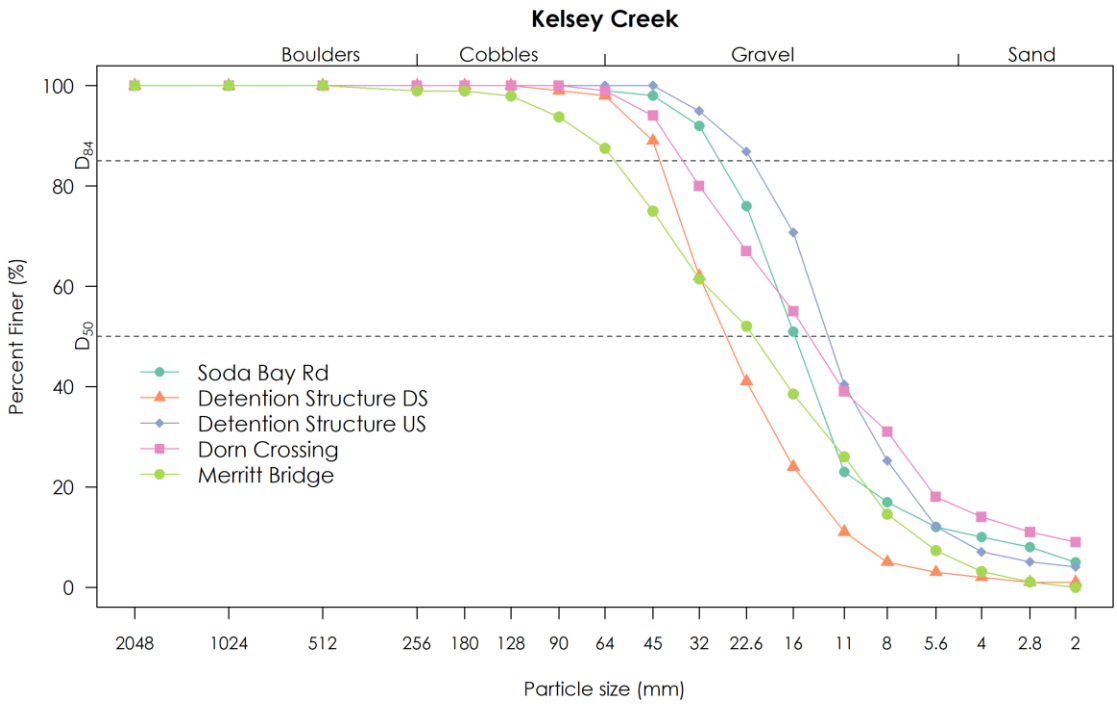

Figure E-6. Particle size distribution in Kelsey Creek with sites ordered downstream to upstream.

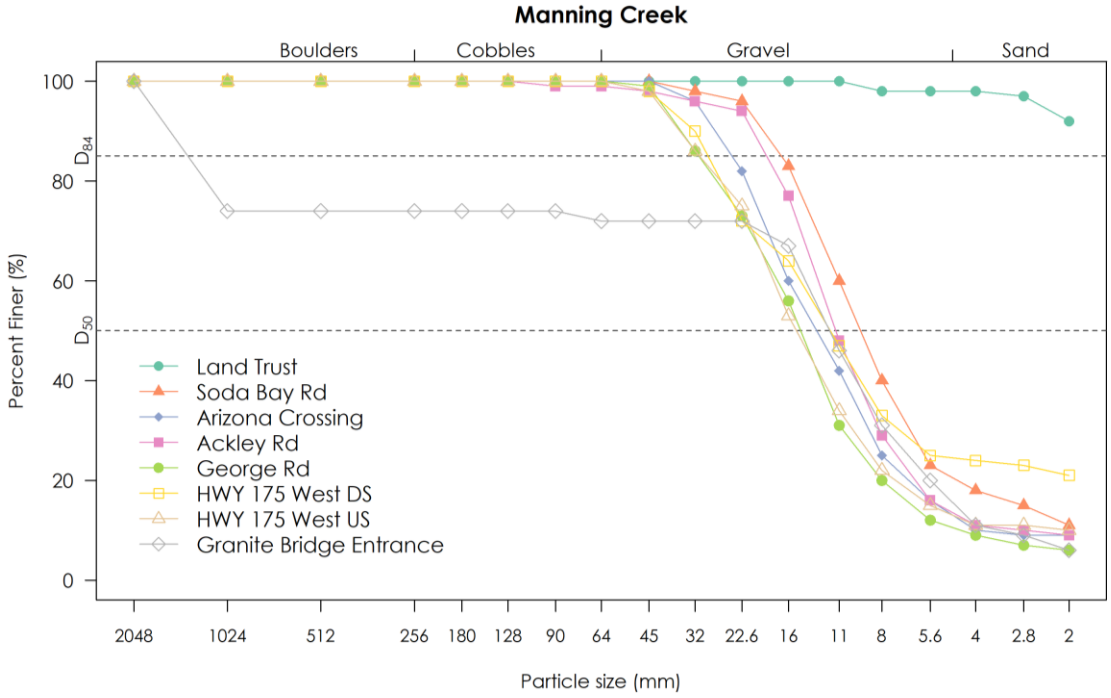

Figure E-7. Particle size distribution in Manning Creek with sites ordered downstream to upstream.

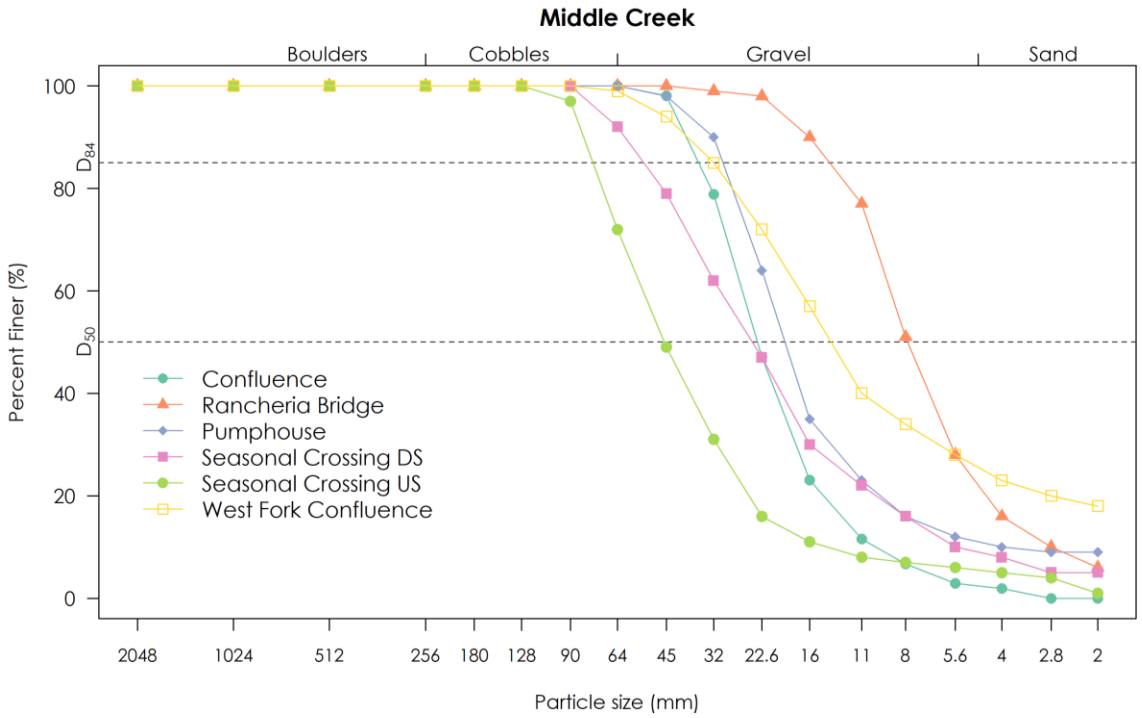

Figure E-8. Particle size distribution in Middle Creek with sites ordered downstream to upstream.

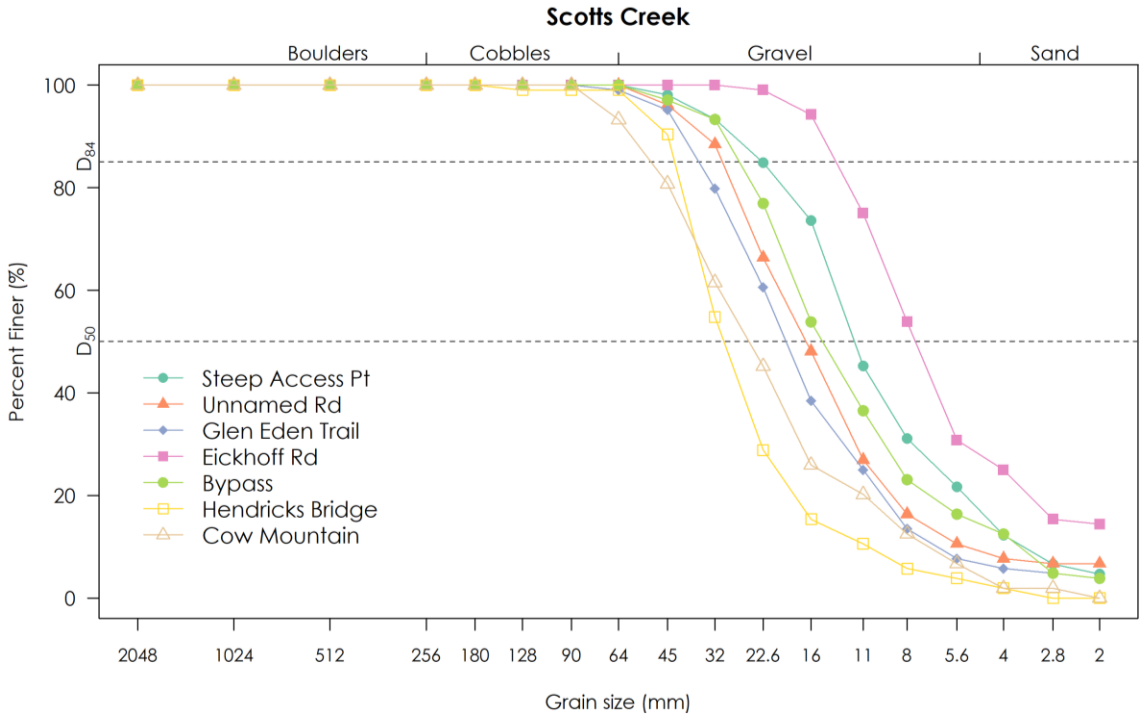

Figure E-9. Particle size distribution in Scotts Creek with sites ordered downstream to upstream.

For 2D model calibration, we averaged the Manning's *n* values calculated from (Bray 1979) for each tributary. The resulting averages (Table E-2) provided the initial starting Manning's *n* for 2D model stage-discharge calibration. The final Manning's *n* values used to calibrate each tributary's 2D model are reported in Table 1, Section 3.2 of the Technical Report. Initial Manning's *n* values were near 0.03 for all tributaries.

Table E-2. Initial Manning's n values used in 2D model calibration. Initial Manning's n values are the average of the n values generated using (Bray 1979) for each tributary.

Tributary Name	Sample Count	Initial Manning's *n* (*n*)
Adobe Creek	9	0.032
Cole Creek	5	0.026
Kelsey Creek	5	0.030
Manning Creek	8	0.026
Middle Creek	6	0.030
Scotts Creek	7	0.029

APPENDIX F: INSTREAM STRUCTURE MEASUREMENTS

F.1 Introduction

Accurate representation of instream structures in a 2D hydraulic model requires precise field measurements of structure dimensions and elevations so they can be integrated into the model domain. Instream structures can include bridges, culverts, flood control structures, fish ladders, and low flow crossings. In 2D HEC-RAS Version 6.5 (USACE 2025) we represented bridges as one-dimensional transects within a 2D Area Connection, including unique bridge elements such as decks, piers, and sloping abutments. Culverts are represented as a combination of weirs and culverts in a 2D Area Connection, while flood control structures and low-flow crossings are represented as weirs in a 2D Area Connection.

F.2 Methods

CDFW used RTK-GPS to record the horizontal locations and elevations of the four pavement notches on the top of the decks. A stadia rod measured deck thickness, which we subtracted from the RTK-GPS elevations to calculate deck bottom elevations. We used a measuring tape to determine the stations of the abutments and piers, relative to the paving notches, while a stadia rod was used to measure the width and length of each pier. For culverts, RTK-GPS units recorded the horizontal locations and elevations of both ends of each culvert's invert, along with the paving notches of the road surface, while a stadia rod was used to measure the diameter of each culvert. We collected data for flood control structures and low flow crossings using RTK-GPS and total station. To ensure consistency, we standardized the collection process, as shown in conceptual graphics (Figures F-1 and F-2). We recorded dimensional measurements and RTK-GPS points on datasheets for later incorporation into HEC-RAS.

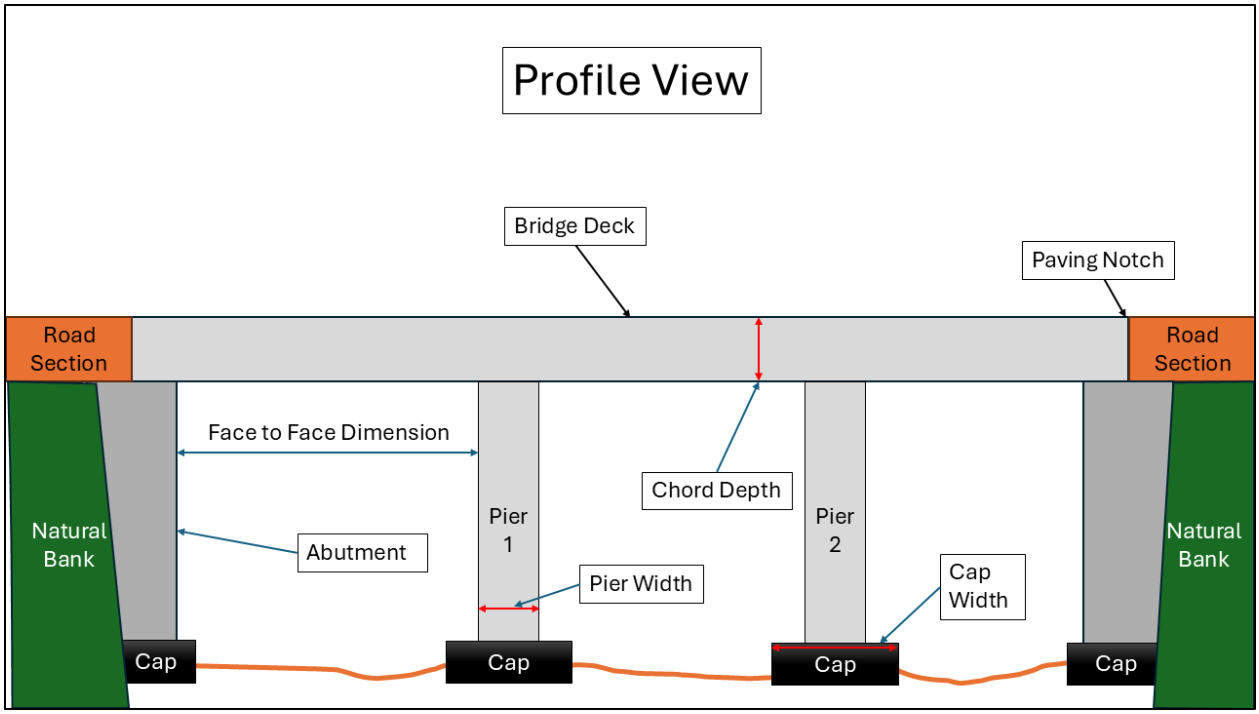

Figure F-1. Conceptual profile view of a bridge structure.

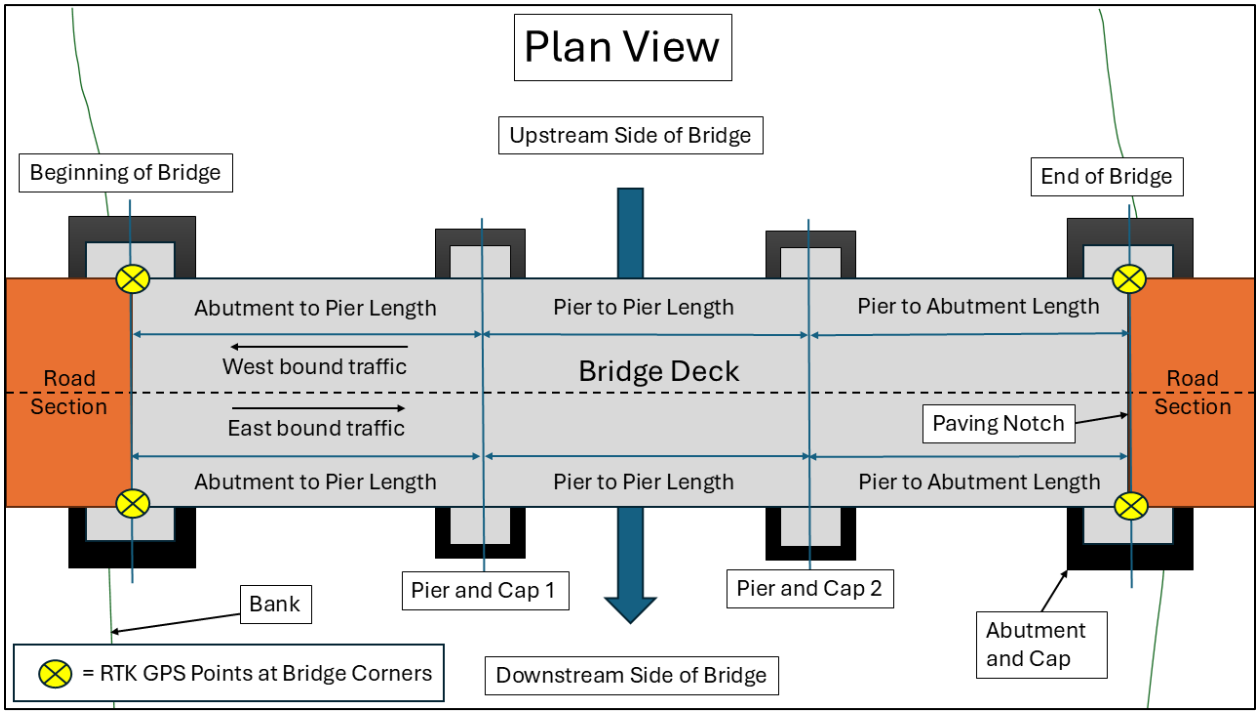

Figure F-2. Conceptual plan view of a bridge structure.

F.3 Results

CDFW conducted a total of 27 bridge structure surveys (Table F-1): five on Adobe, six on Cole, three on Kelsey, five on Manning, three on Middle, and five on Scotts. Figure F-3 is an example of the field data used to generate a bridge structure in the HEC-RAS Connection Data Editor for the bridge spanning Middle Creek at Elk Mountain Road. Additional data was collected to characterize a set of culverts located on Adobe Creek at Bell Hill Road and a flood control structure located on Kelsey Creek near Dorn Crossing.

Table F-1. Instream structure locations by creek and river mile.

Tributary Name	Nearest Location	River Mile
Adobe Creek	Soda Bay Road Bridge	1.9
Adobe Creek	Finley East Road Bridge	2.0
Adobe Creek	Big Valley Road Bridge	2.3
Adobe Creek	Bogert Lane Bridge	2.6
Adobe Creek	Argonaut Road Bridge	2.8
Adobe Creek	Highway 29 Bridge	2.9
Adobe Creek	Bell Hill Road Culverts	5.3
Cole Creek	Soda Bay Road Bridge	1.0
Cole Creek	Jeannie Lane Bridge	1.8
Cole Creek	Clark Drive Bridge	3.2
Cole Creek	Unnamed Road Bridge	3.6
Cole Creek	Sylar Lane Bridge	4.0
Cole Creek	Konocti Road Bridge	4.4
Kelsey Creek	Soda Bay Road Bridge	1.7
Kelsey Creek	Flood Detention Structure	2.8
Kelsey Creek	Merritt Road Bridge	4.0
Kelsey Creek	North Main Street Bridge	4.3
Kelsey Creek	Highway 29 Bridge	4.8
Manning Creek	Soda Bay Road Bridge	1.3
Manning Creek	Arizona Crossing	1.6
Manning Creek	Highway 29 Bridge	2.0
Manning Creek	Ackley Road Bridge	2.7
Manning Creek	George Road Bridge	3.1
Manning Creek	Granite Construction Bridge	4.5
Middle Creek	Highway 20 Bridge	1.1
Middle Creek	Rancheria Road Bridge	2.5
Middle Creek	Elk Mountain Road Bridge	5.5
Scotts Creek	Valley View Road Bridge	6.1
Scotts Creek	Glen Ellen Trailhead Pedestrian Bridge	6.8
Scotts Creek	Unnamed Road Bridge	10.1
Scotts Creek	Eickhoff Road Bridge	12.4
Scotts Creek	Scotts Valley Road Bridge	15.5

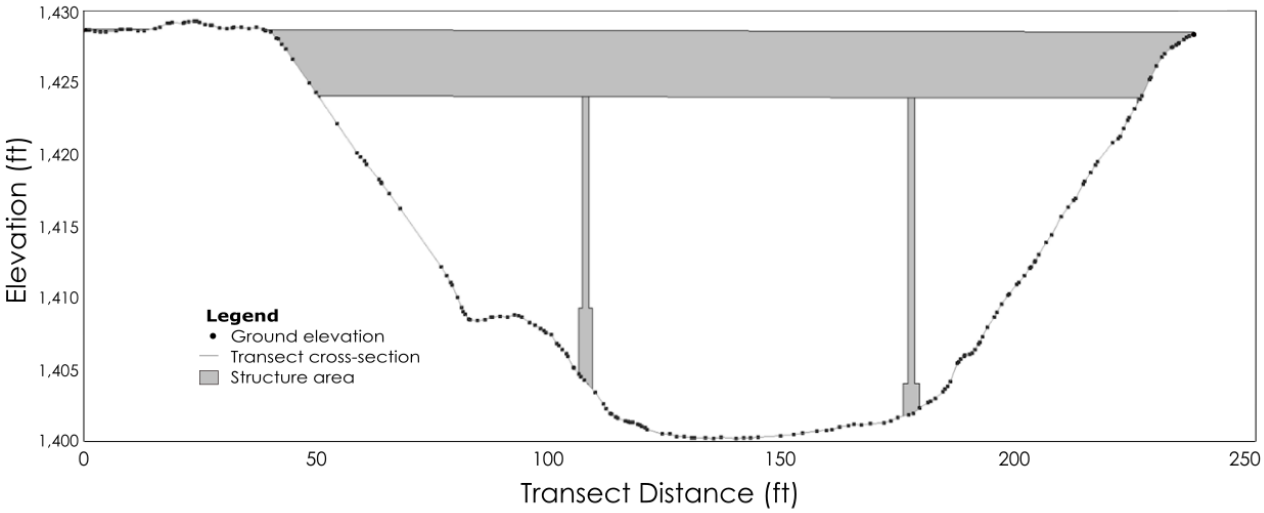

Figure F-3. Upstream view of the Elk Mountain Road Bridge on Middle Creek as visualized in the software HEC-RAS.

APPENDIX G: 2D MODEL CALIBRATION AND VALIDATION

G.1 Introduction

Two-dimensional (2D) hydraulic habitat models were used to assess fish passage conditions within the six study tributaries. The DEM was developed from lidar data (Appendix A) supplemented with additional topographic surveys CDFW conducted to fill voids in the lidar surface (Appendix B). Each DEM was finalized in HEC-RAS by overlaying the void survey data (in raster format) above the green lidar raster for each tributary.

G.2 Methods

CDFW built 2D hydraulic habitat models in HEC-RAS Version 6.5 (USACE 2025) for each of the six tributaries. Flow simulations were run to predict depth and velocity within the defined model boundaries and to identify conditions that could restrict CLH passage. We examined the simulated results to identify potential depth sensitive areas in which the thalweg depth was less than 0.5 ft. Additionally, we looked at velocities from bank to bank that exceeded 5 ft/s as zones that could impede upstream passage.

Each 2D model had a digitized model boundary within the extent of the lidar data. We added a computational mesh for each 2D tributary model area using a grid size of 10 ft, with Surface Area/2D Area connections added to represent bridges and other hydraulic structures. For calibration, we set the upstream and tributary boundary conditions to the measured discharges (Appendix C; Table G-1), while the downstream boundary conditions used normal depth or stage. Note, NA in Table G-1 refers to cases where there were less than three inflow tributaries downstream of the upstream boundary. The initial value of friction slope was calculated from the two downstream-most measured WSEs, and the distance between them. Initial Manning's *n* values came from the pebble count data (see Appendix E). We used the Shallow Water Equations – Eulerian-Lagrangian Method (SWE-ELM) and the conservative turbulence model, with a longitudinal mixing coefficient of 0.3, a lateral mixing coefficient of 0.1, and a Smagorinsky coefficient of 0.05. We ran the HEC-RAS models at the calibration flows listed in Table G-1, followed by a comparison of measured versus simulated WSEs. The Manning's *n* values, and downstream boundary friction slopes or stage were then varied until the simulated WSEs matched the measured WSEs collected in the field (Appendix C; Table C-2).

CDFW measured paired depth and velocity data at multiple locations throughout each study tributary (Appendix D) to validate each 2D model. After each 2D model was calibrated, we ran flow simulations at the flows where

validation data were collected. The HEC-RAS flow simulations produced georeferenced rasters showing depth and velocity across the model domain, which we exported to ArcGIS for mapping.

Table G-1. Calibration flows (cfs).

Tributary	Date	Upstream	Tributary 1	Tributary 2	Tributary 3
Adobe	4/9/2024	20.6	5.67	17.75	NA
Adobe	4/10/2024	15.1	4.1	0	NA
Adobe	4/11/2024	13.9	3.8	0	NA
Cole	4/8/2024	9.8	NA	NA	NA
Cole	4/29/2024	3.5	NA	NA	NA
Cole	5/7/2024	4.4	NA	NA	NA
Kelsey	4/22/2024	49.9	0.6	4.1	NA
Kelsey	4/23/2024	48.9	- 0.9	4.3	NA
Kelsey	4/24/2024	53.3	NA	NA	NA
Kelsey	4/25/2024	48.4	NA	NA	NA
Manning	4/2/2024	8.2	8.4	NA	NA
Manning	4/3/2024	4.3	4.4	NA	NA
Manning	4/4/2024	4.4	4.4	NA	NA
Middle	5/8/2024	14.2	9.1	14.0	10.7
Middle	5/9/2024	12.9	8.3	12.7	9.7
Middle	5/10/2024	13.6	8.7	13.4	10.2
Scotts	5/13/2024	13.6	NA	NA	NA
Scotts	5/14/2024	15.6	NA	NA	NA
Scotts	5/15/2024	20.0	NA	NA	NA
Scotts	5/16/2024	24.5	NA	NA	NA

G.3 Results

Table G-2 gives the final Manning's *n* and friction slope values, along with the mean difference between measured and simulated water surface elevations. For Middle Creek, the downstream boundary condition was best characterized by the water stage (Table G-2) located at the first WSE measured above stage influenced by the lake level, located approximately a quarter-mile downstream of Highway 20 (Figure C-10). Plots of measured versus simulated water surface elevations are shown in Figures G-1 to G-6.

Table G-2. Two-dimensional model calibration results.

Tributary Name	Manning's *n*	Friction Slope/ Stage*	Mean Measured Versus Simulated Water Surface Elevation
Adobe Creek	0.03999	0.0000285	-0.008
Cole Creek	0.010	0.000025	0.019
Kelsey Creek	0.041	0.0000035	0.0003
Lower Manning Creek	0.030	0.000144	0.035
Upper Manning Creek	0.063	0.0001235	0.0084
Middle Creek	0.039	1328.061*	-0.00884
Scotts Creek	0.033	0.000077	0.00

* For Middle Creek, the downstream boundary condition was set to the first measured water surface elevation that was not influenced by lake levels.

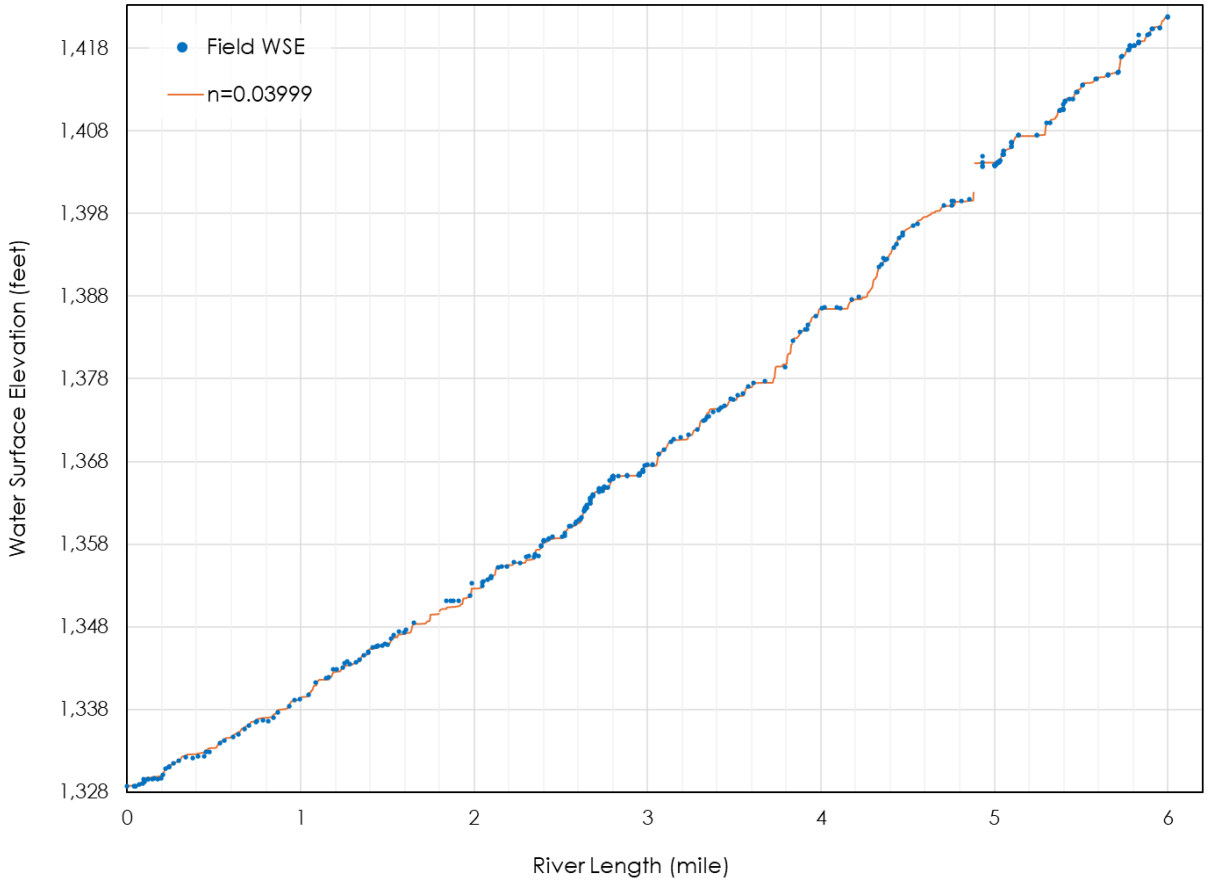

Figure G-1. Adobe Creek simulated and measured water surface elevation profiles.

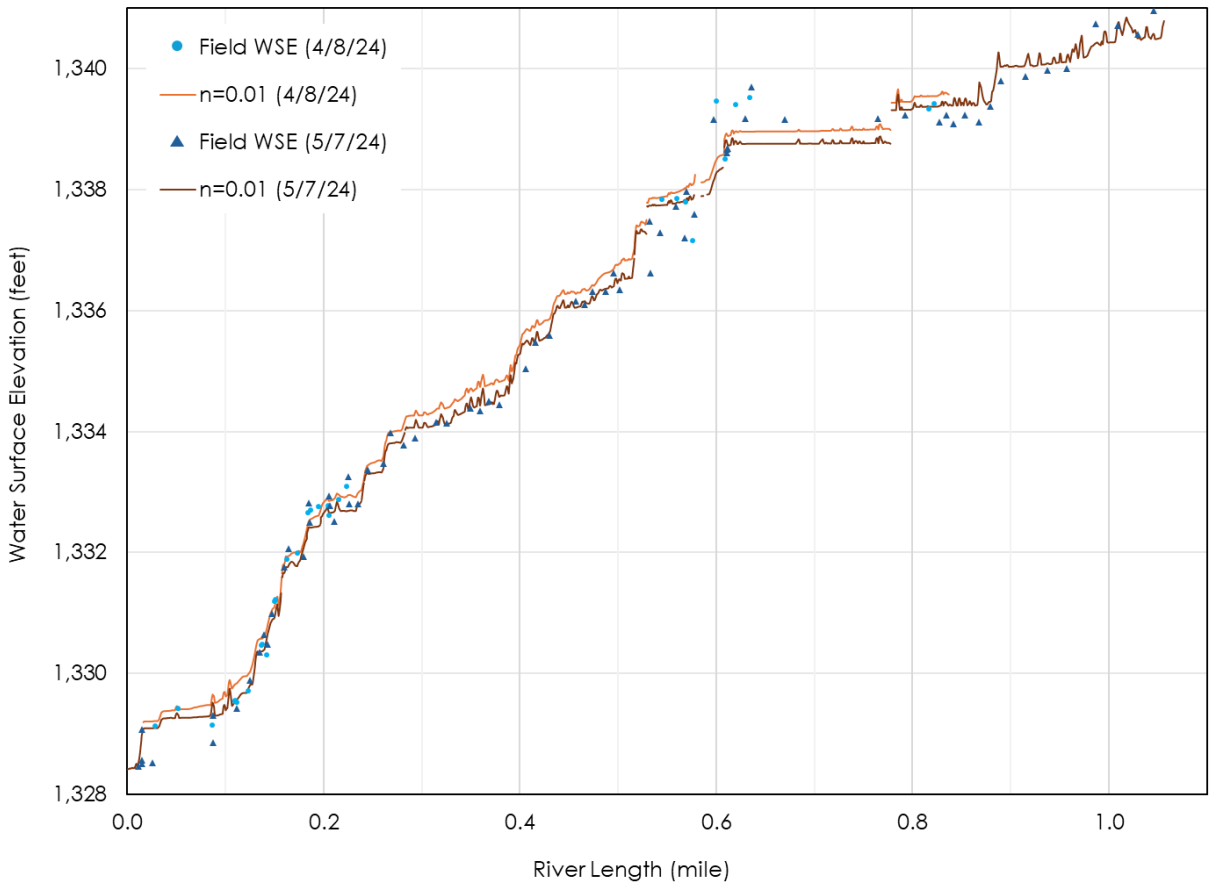

Figure G-2. Cole Creek simulated and measured water surface elevation profiles.

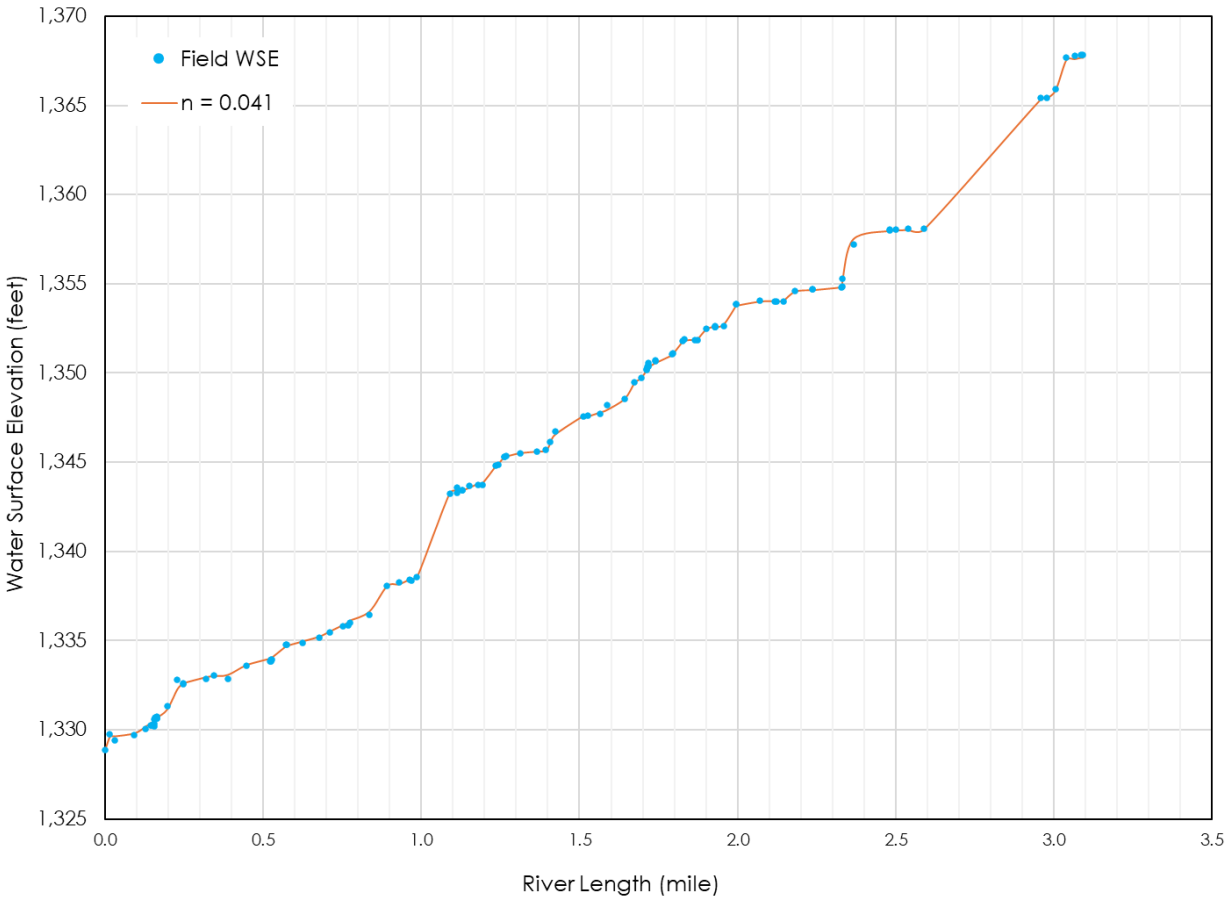

Figure G-3. Kelsey Creek simulated and measured water surface elevation profiles.

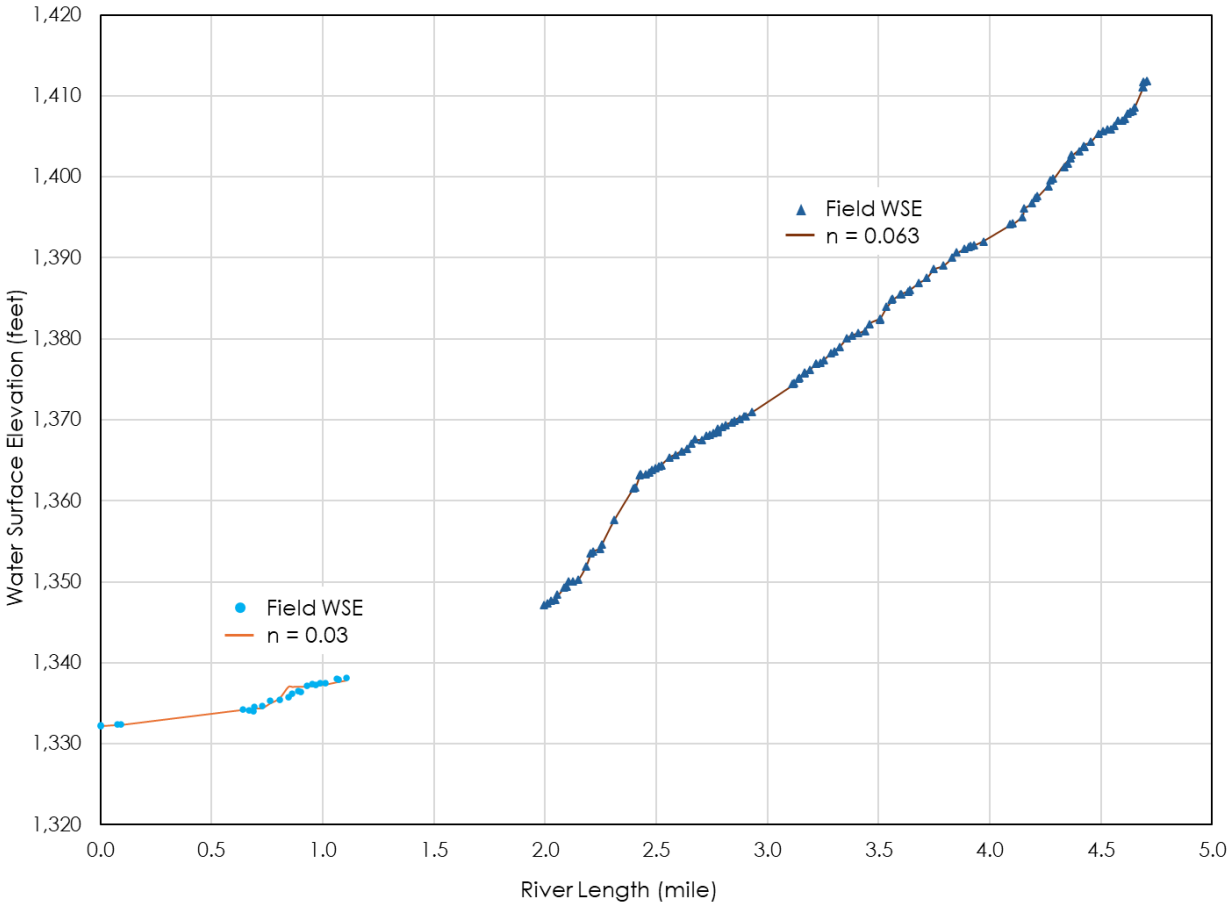

Figure G-4. Manning Creek simulated and measured water surface elevation profiles.

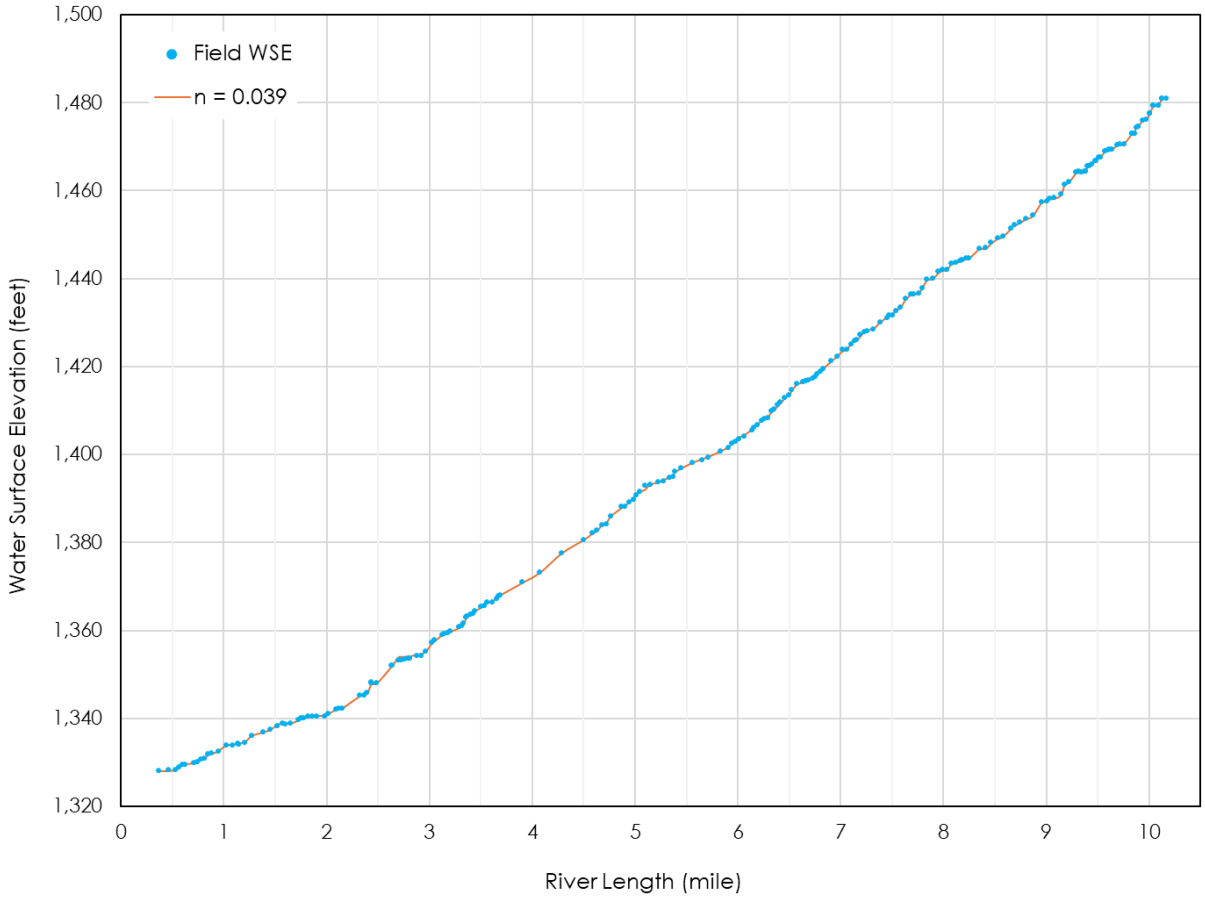

Figure G-5. Middle Creek simulated and measured water surface elevation profiles.

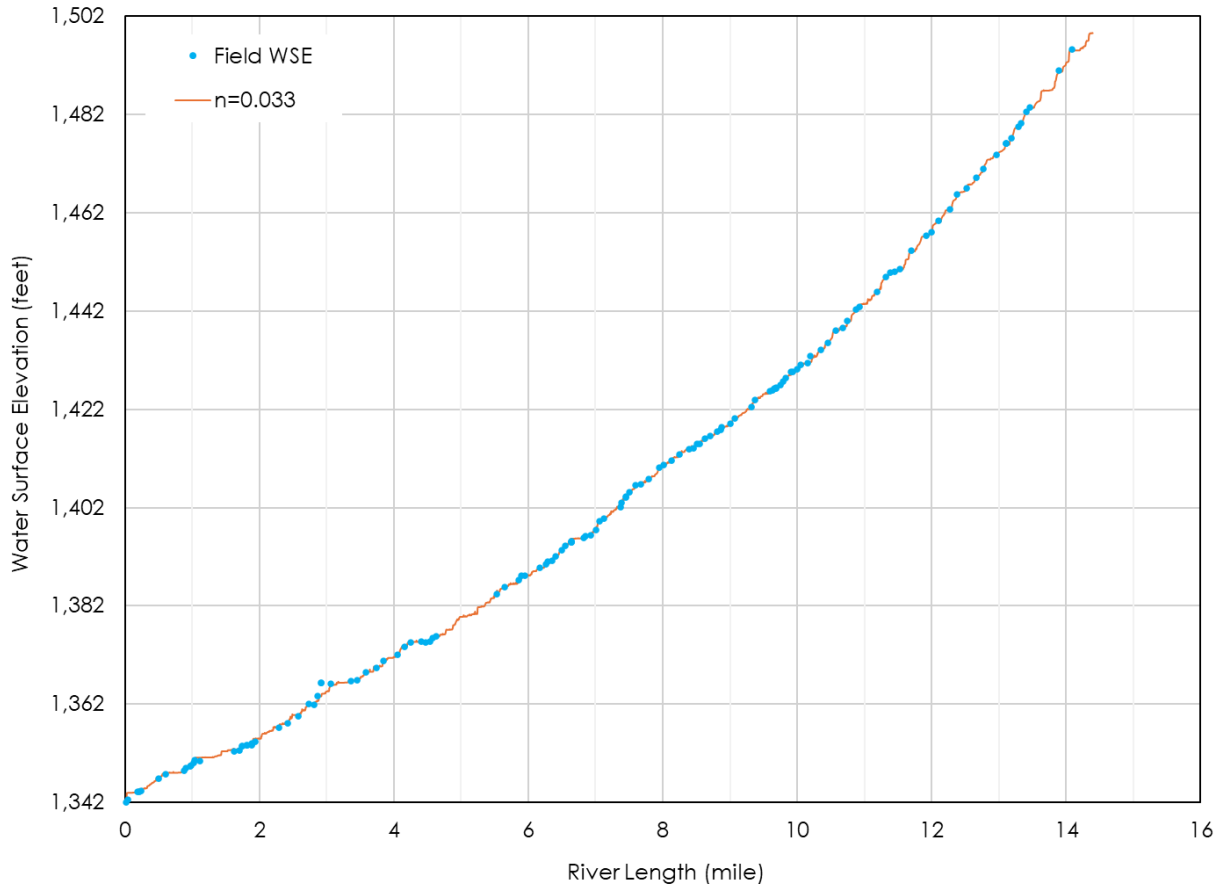

Figure G-6. Scotts Creek simulated and measured water surface elevation profiles.

After 2D model calibration was completed, each model was validated for depth and velocity. When staff collected the WSE-discharge stream profile data for model calibration, depth and velocity validation measurements were collected at randomly chosen locations within the flowing stream of each tributary. The RTK-GPS was used to record a georeferenced location for each validation data point. The validation analysis was executed by performing model simulations at the discharge levels the field validation data were collected under. The simulated depths and velocities were extracted from each tributary model at the georeferenced locations where the field data were collected. In Figure G-7, the depth and velocity validation data collected in the field were plotted with the simulated depths and velocities output from HEC-RAS. The r-squared (R^2) value is reported in each plot. Depth validation R^2 values ranged from 0.55–0.93 and velocity R^2 values ranged from 0.41–0.74.

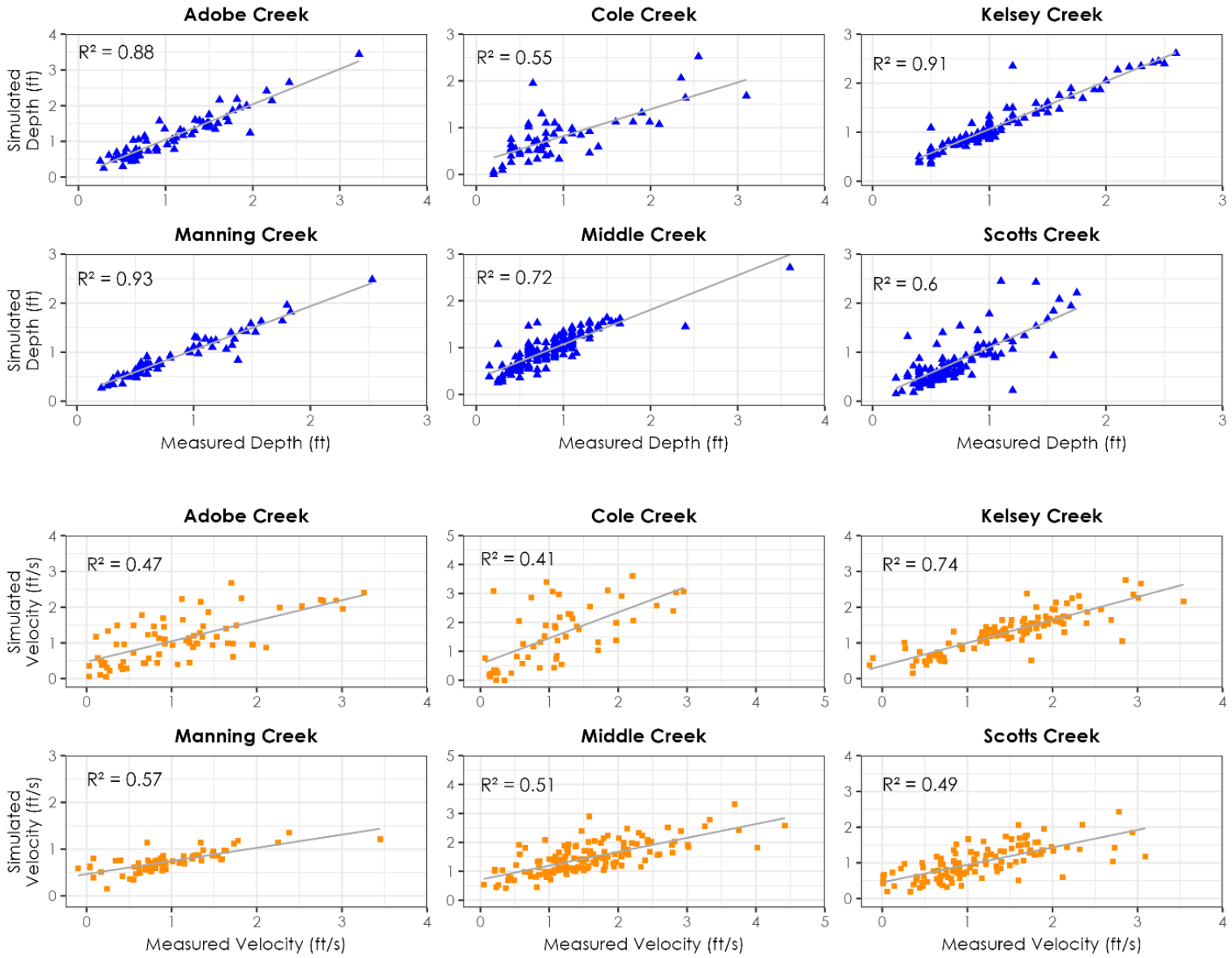

Figure G-7. Depth (blue) and velocity (orange) validation results for each tributary.

In general, the friction slopes at the downstream boundaries were very low, reflecting backwater effects from Clear Lake. The low Manning's *n* value for Cole Creek reflects the very small particle size present in that creek. At these low values, the Cole Creek model was relatively insensitive to changes in the Manning's *n* values, with the mean error dropping from 0.05 ft for the initial Manning's *n* value of 0.018 to 0.019 ft for the final Manning's *n* value of 0.010. While a further decrease in Manning's *n* would have further decreased the mean error, dropping below 0.01 was viewed as unrealistic. Cole Creek showed the largest range of errors, likely reflecting the decreased accuracy of measured water surface elevations in Cole Creek due to heavy tree cover. The large gap in the Adobe Creek water surface elevation profile at Station 25,800 represents the drop in elevation as water flows through the culverts at Bell Hill Road. Manning Creek had two different Manning's *n* values, with the higher value for the upstream reach reflecting additional roughness due to steeper gradients, higher channel sinuosity, and heavy vegetation in the channel.

APPENDIX H: DEPTH SENSITIVE AREAS

H.1 Introduction

In each of the six study tributaries, we used 2D hydraulic modeling to simulate a targeted range of flow conditions for CLH, unique to each creek's hydrology and seasonal flow patterns. We utilized a 0.5-foot minimum depth criterion and a <5 feet per second (ft/s) velocity criterion based on traditional ecological knowledge and prior 2D modeling studies conducted in the Clear Lake watershed (BV EPA 2023). We define areas that do not meet the 0.5-ft depth criterion as DSAs and the most depth sensitive ones as MDSAs.

H.2 Methods

We used the 2D module of HEC-RAS, Version 6.5 (USACE 2025) to estimate depth and velocity across each study tributary to evaluate CLH passage conditions. After model calibration and validation (Appendix G), we set downstream inflow tributary flows to zero to maintain constant flow and simulated a range of discharges within each tributary. Flow simulations were performed at progressively lower flows until thalweg depths less than 0.5 ft indicated which areas were a DSA. We then verified five to seven of the most depth sensitive areas (MDSAs) in the field for each tributary by surveying the shallowest course from bank to bank with the RTK-GPS and measuring the deepest thalweg depth along the shallowest course with a stadia rod.

After completing field verifications of the MDSAs, we applied a three-foot mesh refinement region around each corresponding MDSA within the model domain. The other DSAs were displayed for us to determine the amount of flow needed to maintain passage at the MDSAs. We then re-ran the models with the improved refinement geometries over a range of flows to evaluate whether the depth criterion of 0.5 ft was maintained through the thalweg of each DSA.

H.3 Results

For each tributary, we summarize the location, in river miles, of the assessed DSAs and the water depths for each DSA for a given flow simulation (Tables H-1 through Table H-28). These tables include MDSAs and report water depth with respect to the thalweg across the shallowest course for each DSA at specific simulated flows.

Table H-1. Depth sensitive areas and most depth sensitive areas in Adobe Creek by river mile; bold rows with an asterisk (*) denote most depth sensitive areas.

Depth Sensitive Area Identifier	River Mile
AD-DSA-1	1.2
AD-DSA-2	1.9
AD-DSA-3	2.6
AD-DSA-4	4.6
AD-DSA-5	4.6
AD-DSA-6	4.6
AD-DSA-7	4.7
AD-MDSA-8*	**4.7***
AD-DSA-9	4.8
AD-DSA-10	4.8
AD-DSA-11	5.1
AD-DSA-12	5.1
AD-DSA-13	5.2
AD-DSA-14	5.2
AD-MDSA-15*	**5.2***
AD-MDSA-16*	**5.2***
AD-DSA-17	5.5
AD-MDSA-18*	**6.0***
AD-MDSA-19*	**6.1***
AD-DSA-20	6.2

Table H-2. Depth sensitive areas and most depth sensitive areas 1–15 identified in Adobe Creek with simulated flows and depth outputs. Depths less than 0.5 ft are shown in bold and marked with a hashtag (#) symbol.

Flow (cfs)	AD-DSA-1	AD-DSA-2	AD-DSA-3	AD-DSA-4	AD-DSA-5	AD-MDSA-8	AD-MDSA-15
10	**0.13#**	**0.04#**	NA	NA	NA	**0.28#**	**0.28#**
12.5	**0.16#**	**0.10#**	NA	NA	NA	**0.31#**	**0.30#**
20	**0.26#**	**0.28#**	NA	NA	NA	**0.39#**	**0.35#**
34	**0.47#**	**0.49#**	**0.40#**	**0.47#**	**0.47#**	**0.49#**	**0.35#**
36	**0.49#**	0.51	**0.43#**	0.50	**0.48#**	0.50	**0.37#**
38	0.51	0.54	**0.46#**	0.52	0.50	0.52	**0.40#**
40	0.53	0.57	**0.49#**	0.55	0.51	0.53	**0.42#**
45	0.59	0.66	0.56	0.60	0.55	0.56	**0.48#**
47	0.61	0.69	0.58	0.62	0.56	0.57	0.50
50	0.65	0.74	0.60	0.64	0.58	0.58	0.53
52	0.67	0.77	NA	NA	NA	0.59	0.55
55	0.71	0.82	NA	NA	NA	0.61	0.59
60	0.77	0.90	NA	NA	NA	0.62	0.65
70	0.88	1.03	NA	NA	NA	0.67	0.78
74	0.93	1.09	NA	NA	NA	0.69	0.82

Table H-3. Most depth sensitive areas 16–19 identified in Adobe Creek with simulated flows and depth outputs. Depths less than 0.5 ft are shown in bold and marked with a hashtag (#) symbol.

Flow (cfs)	AD-MDSA-16	AD-MDSA-18	AD-MDSA-19
10	**0.32#**	**0.39#**	**0.32#**
12.5	**0.34#**	**0.41#**	**0.35#**
20	**0.38#**	**0.47#**	**0.42#**
34	**0.43#**	0.53	0.52
36	**0.44#**	0.53	0.53
38	**0.44#**	0.54	0.55
40	**0.45#**	0.54	0.56
45	**0.46#**	0.55	0.58
47	**0.47#**	0.55	0.59
50	**0.48#**	0.56	0.60
52	0.50	0.57	0.61
55	0.52	0.58	0.62
60	0.55	0.59	0.64
70	0.59	0.62	0.68
74	0.61	0.63	0.70

Table H-4. Depth sensitive areas and most depth sensitive areas in Cole Creek by river mile; bold rows with an asterisk (*) denote most depth sensitive areas.

Depth Sensitive Area Identifier	River Mile
CO-MDSA-7*	**1.1***
CO-DSA-9	1.2
CO-MDSA-14*	**1.4***
CO-DSA-15	1.4
CO-MDSA-16*	**1.4***
CO-MDSA-17*	**1.5***
CO-MDSA-19*	**1.5***
CO-DSA-47	2.7
CO-MDSA-84*	**3.9***
CO-DSA-88	4.1
CO-DSA-97	4.3

Table H-5. Depth sensitive areas and most depth sensitive areas 7–17 identified in Cole Creek with simulated flows and depth outputs. Depths less than 0.5 ft are shown in bold and marked with a hashtag (#) symbol.

Flow (cfs)	CO-MDSA-7	CO-DSA-9	CO-MDSA-14	CO-DSA-15	CO-MDSA-16	CO-MDSA-17
9.8	**0.19#**	**0.24#**	**0.13#**	**0.31#**	**0.17#**	**0.21#**
16.5	**0.37#**	NA	**0.30#**	NA	**0.33#**	**0.33#**
20	**0.47#**	NA	**0.39#**	NA	**0.41#**	**0.39#**
21.5	0.50	NA	**0.40#**	NA	**0.42#**	**0.40#**
23	0.52	NA	**0.41#**	NA	**0.43#**	**0.40#**
25	0.56	NA	**0.43#**	NA	**0.45#**	**0.41#**
30	0.64	0.65	**0.48#**	0.62	**0.49#**	**0.42#**
31	0.66	NA	**0.49#**	NA	0.50	**0.42#**
32	0.67	NA	0.50	NA	0.51	**0.42#**
35	0.72	NA	0.52	NA	0.53	**0.42#**
38	0.77	NA	0.55	NA	0.56	**0.44#**
50	1.25	NA	0.68	NA	0.65	**0.44#**
70	1.29	NA	0.90	NA	0.76	**0.45#**
89	1.53	NA	1.12	NA	0.87	0.50
100	1.67	NA	1.25	NA	0.94	0.53

Table H-6. Depth sensitive areas and most depth sensitive areas 19–97 identified in Cole Creek with simulated flows and depth outputs. Depths less than 0.5 ft are shown in bold and marked with a hashtag (#) symbol.

Flow (cfs)	CO-MDSA-19	CO-DSA-47	CO-MDSA-84	CO-DSA-88	CO-DSA-97
9.8	**0.12#**	**0.32#**	**0.16#**	**0.29#**	**0.32#**
16.5	**0.34#**	NA	**0.31#**	NA	NA
20	**0.46#**	NA	**0.39#**	NA	NA
21.5	**0.48#**	NA	**0.41#**	NA	NA
23	0.50	NA	**0.42#**	NA	NA
25	0.53	NA	**0.44#**	NA	NA
30	0.58	0.59	**0.49#**	0.63	0.59
31	0.59	NA	0.50	NA	NA
32	0.60	NA	0.51	NA	NA
35	0.64	NA	0.54	NA	NA
38	0.67	NA	0.57	NA	NA
50	0.78	NA	0.69	NA	NA
70	0.89	NA	0.85	NA	NA
89	0.97	NA	1.03	NA	NA
100	1.01	NA	1.14	NA	NA

Table H-7. Depth sensitive areas and most depth sensitive areas in Kelsey Creek by river mile; bold rows with an asterisk (*) denote most depth sensitive areas.

Depth Sensitive Area Identifier	River Mile
KE-MDSA-1*	**2.3***
KE-MDSA-2*	**2.9***
KE-MDSA-3*	**3.1***
KE-MDSA-4*	**3.4***
KE-MDSA-5*	**3.7***
KE-MDSA-6*	**4.0***
KE-DSA-7	1.7
KE-DSA-8	1.7
KE-DSA-9	1.9
KE-DSA-10	1.9
KE-DSA-11	2.0
KE-DSA-12	2.0
KE-DSA-13	2.1
KE-DSA-14	2.3
KE-DSA-15	2.4
KE-DSA-16	2.5
KE-DSA-17	2.6
KE-DSA-18	2.7
KE-DSA-19	2.9
KE-DSA-20	3.1
KE-DSA-21	3.2
KE-DSA-22	3.3
KE-DSA-23	3.4
KE-DSA-24	3.6
KE-DSA-25	3.7
KE-DSA-26	3.7
KE-DSA-27	4.0
KE-DSA-28	4.1
KE-DSA-29	4.5
KE-DSA-30	4.7
KE-DSA-31	4.7

Table H-8. Depth sensitive areas and most depth sensitive areas 1–7 identified in Kelsey Creek with simulated flows and depth outputs. Depths less than 0.5 ft are shown in bold and marked with a hashtag (#) symbol.

Flow (cfs)	KE-MDSA-1	KE-MDSA-2	KE-MDSA-3	KE-MDSA-4	KE-MDSA-5	KE-MDSA-6	KE-DSA-7
10	**0.26#**	**0.12#**	**0.17#**	**0.22#**	**0.26#**	**0.21#**	**0.27#**
20	**0.38#**	**0.20#**	**0.25#**	**0.32#**	**0.40#**	**0.35#**	0.61
30	**0.48#**	**0.34#**	**0.33#**	**0.43#**	**0.49#**	**0.44#**	0.65
40	0.57	**0.35#**	**0.41#**	0.50	0.58	0.52	0.95
50	0.66	**0.37#**	**0.49#**	0.55	0.66	0.60	1.32
60	0.76	**0.42#**	0.56	0.61	0.73	0.66	1.72
70	0.86	0.50	0.63	0.66	0.81	0.73	2.09
80	0.96	0.57	0.69	0.72	0.89	0.78	2.44

Table H-9. Depth sensitive areas 8–14 identified in Kelsey Creek with simulated flows and depth outputs. Depths less than 0.5 ft are shown in bold and marked with a hashtag (#) symbol.

Flow (cfs)	KE-DSA-8	KE-DSA-9	KE-DSA-10	KE-DSA-11	KE-DSA-12	KE-DSA-13	KE-DSA-14
10	**0.35#**	**0.31#**	**0.46#**	**0.30#**	**0.43#**	**0.42#**	**0.39#**
20	0.52	0.62	0.68	0.50	0.62	0.59	0.57
30	0.68	0.76	0.83	0.67	0.77	0.75	0.73
40	0.84	0.99	0.96	0.80	0.89	0.91	0.89
50	1.04	1.11	1.08	0.93	1.01	1.05	1.03
60	1.29	1.31	1.19	1.04	1.12	1.19	1.17
70	1.58	1.48	1.29	1.15	1.22	1.32	1.29
80	1.89	1.70	1.38	1.25	1.31	1.44	1.42

Table H-10. Depth sensitive areas 15–21 identified in Kelsey Creek with simulated flows and depth outputs. Depths less than 0.5 ft are shown in bold and marked with a hashtag (#) symbol.

Flow (cfs)	KE-DSA-15	KE-DSA-16	KE-DSA-17	KE-DSA-18	KE-DSA-19	KE-DSA-20	KE-DSA-21
10	**0.31#**	**0.41#**	**0.41#**	**0.31#**	**0.35#**	0.53	**0.32#**
20	**0.48#**	0.60	0.54	**0.48#**	0.51	0.79	**0.44#**
30	0.62	0.76	0.67	0.63	0.72	0.98	0.54
40	0.76	0.91	0.78	0.77	0.84	1.13	0.63
50	0.88	1.05	0.89	0.89	0.94	1.27	0.71
60	1.00	1.18	0.98	1.00	1.02	1.39	0.78
70	1.11	1.31	1.07	1.10	1.10	1.49	0.85
80	1.21	1.42	1.15	1.20	1.17	1.58	0.91

Table H-11. Depth sensitive areas 22–28 identified in Kelsey Creek with simulated flows and depth outputs. Depths less than 0.5 ft are shown in bold and marked with a hashtag (#) symbol.

Flow (cfs)	KE-DSA-22	KE-DSA-23	KE-DSA-24	KE-DSA-25	KE-DSA-26	KE-DSA-27	KE-DSA-28
10	**0.40#**	**0.43#**	**0.30#**	**0.33#**	**0.32#**	**0.32#**	**0.32#**
20	0.56	0.60	**0.43#**	0.50	**0.41#**	**0.47#**	**0.49#**
30	0.73	0.72	0.57	0.61	0.50	0.61	0.62
40	0.89	0.82	0.69	0.72	0.59	0.73	0.73
50	1.04	0.90	0.80	0.83	0.68	0.85	0.83
60	1.18	0.97	0.91	0.94	0.76	0.95	0.92
70	1.31	1.04	1.01	1.04	0.84	1.06	1.00
80	1.43	1.10	1.11	1.14	0.90	1.15	1.07

Table H-12. Depth sensitive areas 29–31 identified in Kelsey Creek with simulated flows and depth outputs. Depths less than 0.5 ft are shown in bold and marked with a hashtag (#) symbol.

Flow (cfs)	KE-DSA-29	KE-DSA-30	KE-DSA-31
10	**0.31#**	**0.31#**	**0.36#**
20	**0.47#**	0.52	**0.47#**
30	0.57	0.61	0.57
40	0.68	0.74	0.66
50	0.78	0.91	0.74
60	0.86	1.01	0.81
70	0.94	1.12	0.87
80	1.02	1.24	0.94

Table H-13. Depth sensitive areas and most depth sensitive areas 0–33 in Manning Creek by river mile; bold rows with an asterisk (*) denote most depth sensitive areas.

Depth Sensitive Area Identifier	River Mile
MA-DSA-0	1.2
MA-DSA-1	1.3
MA-DSA-2	1.5
MA-DSA-3	1.5
MA-DSA-4	1.6
MA-DSA-5	2.3
MA-MDSA-6*	**2.3***
MA-DSA-7	2.3
MA-DSA-8	2.4
MA-DSA-9	2.4
MA-DSA-10	2.4
MA-MDSA-11*	**2.4***
MA-MDSA-12*	**2.5***
MA-DSA-13	2.8
MA-DSA-14	2.9
MA-DSA-15	3.4
MA-DSA-16	3.5
MA-MDSA-17*	**3.6***
MA-DSA-18	3.6
MA-DSA-19	3.6
MA-DSA-20	3.7
MA-DSA-21	3.7
MA-DSA-22	3.8
MA-DSA-23	4.2
MA-DSA-24	4.2
MA-MDSA-25*	**4.3***
MA-DSA-26	4.5
MA-DSA-27	4.6
MA-DSA-28	4.6
MA-DSA-29	4.6
MA-DSA-30	4.6
MA-DSA-31	4.6
MA-DSA-32	2.5
MA-DSA-33	2.7

Table H-14. Depth sensitive areas 34–38 in Manning Creek by river mile.

Depth Sensitive Area Identifier	River Mile
MA-DSA-34	2.8
MA-DSA-35	4.3
MA-DSA-36	4.4
MA-DSA-37	1.5
MA-DSA-38	1.6

Table H-15. Depth sensitive areas and most depth sensitive areas 0–6 identified in Manning Creek with simulated flows and depth outputs. Depths less than 0.5 ft are shown in bold and marked with a hashtag (#) symbol.

Flow (cfs)	MA-DSA-0	MA-DSA-1	MA-DSA-2	MA-DSA-3	MA-DSA-4	MA-DSA-5	MA-MDSA-6
5	**0.34#**	**0.33#**	**0.30#**	**0.28#**	**0.24#**	**0.20#**	**0.20#**
10	0.53	0.50	**0.47#**	**0.46#**	**0.40#**	**0.38#**	**0.33#**
15	0.70	0.63	0.61	0.65	0.54	0.55	**0.41#**
20	0.88	0.77	0.72	0.77	0.68	0.67	**0.48#**
25	0.98	0.89	0.84	0.91	0.80	0.70	0.54
30	1.12	1.01	0.95	1.03	0.92	0.90	0.60

Table H-16. Depth sensitive areas 7–12 identified in Manning Creek with simulated flows and depth outputs. Depths less than 0.5 ft are shown in bold and marked with a hashtag (#) symbol.

Flow (cfs)	MA-DSA-7	MA-DSA-8	MA-DSA-9	MA-DSA-10	MA-MDSA-11	MA-MDSA-12
5	**0.29#**	**0.29#**	**0.21#**	**0.21#**	**0.27#**	**0.16#**
10	**0.47#**	**0.41#**	**0.38#**	**0.34#**	**0.36#**	**0.27#**
15	0.61	0.58	0.51	**0.46#**	**0.41#**	**0.36#**
20	0.73	0.59	0.62	0.57	**0.46#**	**0.42#**
25	0.83	0.60	0.72	0.66	0.52	0.50
30	0.93	0.64	0.81	0.75	0.59	0.57

Table H-17. Depth sensitive areas and most depth sensitive areas 13–19 identified in Manning Creek with simulated flows and depth outputs. Depths less than 0.5 ft are shown in bold and marked with a hashtag (#) symbol.

Flow (cfs)	MA-DSA-13	MA-DSA-14	MA-DSA-15	MA-DSA-16	MA-MDSA-17	MA-DSA-18	MA-DSA-19
5	**0.23#**	**0.21#**	**0.31#**	**0.27#**	**0.19#**	**0.28#**	**0.26#**
10	**0.36#**	**0.47#**	**0.40#**	**0.41#**	**0.33#**	**0.42#**	**0.40#**
15	**0.47#**	0.65	0.57	0.53	**0.42#**	0.52	0.53
20	0.58	0.81	0.68	0.64	**0.49#**	0.62	0.64
25	0.68	0.95	0.77	0.75	0.56	0.71	0.74
30	0.78	1.08	0.87	0.85	0.61	0.79	0.83

Table H-18. Depth sensitive areas and most depth sensitive areas 20–25 identified in Manning Creek with simulated flows and depth outputs. Depths less than 0.5 ft are shown in bold and marked with a hashtag (#) symbol.

Flow (cfs)	MA-DSA-20	MA-DSA-21	MA-DSA-22	MA-DSA-23	MA-DSA-24	MA-MDSA-25
5	**0.29#**	**0.21#**	**0.25#**	**0.16#**	**0.34#**	**0.15#**
10	**0.42#**	**0.38#**	**0.34#**	**0.35#**	0.50	**0.28#**
15	0.56	0.50	**0.43#**	0.51	0.64	**0.41#**
20	0.68	0.62	0.50	0.67	0.77	**0.46#**
25	0.81	0.73	0.58	0.80	0.88	**0.49#**
30	0.91	0.84	0.66	0.93	1.00	0.52

Table H-19. Depth sensitive areas 26–32 identified in Manning Creek with simulated flows and depth outputs. Depths less than 0.5 ft are shown in bold and marked with a hashtag (#) symbol.

Flow (cfs)	MA-DSA-26	MA-DSA-27	MA-DSA-28	MA-DSA-29	MA-DSA-30	MA-DSA-31	MA-DSA-32
5	**0.33#**	**0.46#**	**0.39#**	**0.25#**	**0.34#**	**0.38#**	**0.29#**
10	**0.49#**	0.67	0.64	**0.48#**	**0.46#**	0.50	0.51
15	0.63	0.84	0.84	0.70	0.55	0.57	0.70
20	0.75	0.98	1.02	0.88	0.63	0.63	0.85
25	0.86	1.12	1.16	1.08	0.68	0.69	0.98
30	0.96	1.23	1.29	1.20	0.73	0.75	1.10

Table H-20. Depth sensitive areas 33–38 identified in Manning Creek with simulated flows and depth outputs. Depths less than 0.5 ft are shown in bold and marked with a hashtag (#) symbol.

Flow (cfs)	MA-DSA-33	MA-DSA-34	MA-DSA-35	MA-DSA-36	MA-DSA-37	MA-DSA-38
5	**0.35#**	**0.28#**	**0.31#**	**0.29#**	**0.29#**	**0.32#**
10	0.51	0.50	0.51	**0.48#**	**0.45#**	0.51
15	0.67	0.67	0.67	0.63	0.58	0.67
20	0.81	0.82	0.81	0.77	0.69	0.81
25	0.92	0.95	0.93	0.88	0.80	0.94
30	1.07	1.07	1.04	0.99	0.90	1.06

Table H-21. Depth sensitive areas and most depth sensitive areas 0–30 in Middle Creek by river mile; bold rows with an asterisk (*) denote most depth sensitive areas.

Depth Sensitive Area Identifier	River Mile
MI-DSA-0	3.2
MI-DSA-1	2.4
MI-DSA-2	2.3
MI-DSA-3	2.1
MI-MDSA-4*	**2.5***
MI-DSA-5	3.5
MI-DSA-6	4.0
MI-DSA-7	4.4
MI-DSA-8	4.6
MI-DSA-9	4.7
MI-DSA-10	4.9
MI-DSA-11	5.0
MI-DSA-12	6.0
MI-DSA-13	6.1
MI-DSA-14	6.2
MI-DSA-15	6.5
MI-DSA-16	6.6
MI-DSA-17	6.6
MI-MDSA-18*	**6.8***
MI-DSA-19	7.2
MI-DSA-20	7.2
MI-MDSA-21*	**7.4***
MI-DSA-22	7.5
MI-DSA-23	7.6
MI-DSA-24	7.7
MI-DSA-25	7.8
MI-DSA-26	7.9
MI-DSA-27	8.0
MI-DSA-28	8.1
MI-DSA-29	8.2
MI-MDSA-30*	**8.4***

Table H-22. Depth sensitive areas and most depth sensitive areas 31–58 in Middle Creek by river mile; bold rows with an asterisk (*) denote most depth sensitive areas.

Depth Sensitive Area Identifier	River Mile
MI-DSA-31	8.7
MI-DSA-32	8.7
MI-DSA-33	8.8
MI-DSA-34	9.0
MI-DSA-35	9.1
MI-DSA-36	9.2
MI-DSA-37	9.2
MI-DSA-38	9.3
MI-DSA-39	9.3
MI-DSA-40	9.4
MI-MDSA-41*	**9.4***
MI-MDSA-42*	**9.5***
MI-DSA-43	9.6
MI-DSA-44	9.6
MI-DSA-45	9.7
MI-DSA-46	9.7
MI-DSA-47	9.7
MI-DSA-48	9.8
MI-DSA-49	9.9
MI-DSA-50	10.0
MI-DSA-51	10.0
MI-DSA-52	10.1
MI-DSA-53	10.1
MI-DSA-54	10.2
MI-DSA-55	10.3
MI-DSA-56	10.3
MI-DSA-57	10.3
MI-DSA-58	10.4

Table H-23. Depth sensitive areas and most depth sensitive areas 4–30 identified in Middle Creek with simulated flows and depth outputs. Depths less than 0.5 ft are shown in bold and marked with a hashtag (#) symbol.

Flow (cfs)	MI-MDSA-4	MI-MDSA-18	MI-DSA-19	MI-MDSA-21	MI-DSA-27	MI-MDSA-30
10	**0.03#**	**0.00#**	**0.22#**	**0.16#**	**0.11#**	**0.05#**
20	**0.15#**	**0.10#**	**0.34#**	**0.21#**	**0.20#**	**0.14#**
30	**0.36#**	**0.21#**	**0.37#**	**0.26#**	**0.29#**	**0.27#**
40	**0.44#**	**0.31#**	**0.42#**	**0.30#**	**0.35#**	**0.37#**
50	0.51	**0.39#**	0.50	**0.35#**	**0.39#**	**0.41#**
60	0.58	**0.41#**	0.58	**0.39#**	**0.49#**	**0.46#**
70	0.64	**0.45#**	0.63	**0.43#**	0.55	0.51
80	0.70	0.50	0.69	**0.46#**	0.60	0.55
90	0.77	0.55	0.74	0.50	0.66	0.60
100	0.82	0.60	0.79	0.53	0.73	0.63

Table H-24. Depth sensitive areas and most depth sensitive areas 35–48 identified in Middle Creek with simulated flows and depth outputs. Depths less than 0.5 ft are shown in bold and marked with a hashtag (#) symbol.

Flow (cfs)	MI-DSA-35	MI-MDSA-41	MI-MDSA-42	MI-DSA-47	MI-DSA-48
10	**0.11#**	**0.25#**	**0.15#**	**0.18#**	**0.22#**
20	**0.19#**	**0.32#**	**0.27#**	**0.26#**	**0.28#**
30	**0.26#**	**0.36#**	**0.31#**	**0.31#**	**0.32#**
40	**0.36#**	**0.39#**	**0.38#**	**0.38#**	**0.40#**
50	**0.42#**	**0.42#**	**0.43#**	**0.46#**	**0.47#**
60	0.54	**0.45#**	**0.47#**	0.54	0.50
70	0.61	**0.47#**	0.51	0.63	0.54
80	0.67	0.50	0.56	0.70	0.59
90	0.74	0.52	0.62	0.77	0.63
100	0.80	0.55	0.68	0.83	0.68

Table H-25. Depth sensitive areas and most depth sensitive areas 1–31 in Scotts Creek by river mile; bold rows with an asterisk (*) denote most depth sensitive areas.

Depth Sensitive Area Identifier	River Mile
SC-DSA-1	6.1
SC-MDSA-2*	**7.0***
SC-DSA-3	7.0
SC-DSA-4	7.3
SC-DSA-5	8.8
SC-DSA-6	9.8
SC-DSA-7	10.0
SC-DSA-8	10.6
SC-DSA-9	11.0
SC-DSA-10	11.2
SC-DSA-11	11.5
SC-DSA-12	11.9
SC-DSA-13	13.5
SC-DSA-14	13.8
SC-DSA-15	14.1
SC-DSA-16	14.8
SC-DSA-17	15.0
SC-DSA-18	15.4
SC-DSA-19	15.7
SC-DSA-20	15.8
SC-DSA-21	16.0
SC-DSA-22	16.2
SC-DSA-23	16.3
SC-DSA-24	16.6
SC-DSA-25	16.7
SC-DSA-26	16.8
SC-DSA-27	16.9
SC-DSA-28	16.9
SC-DSA-29	17.0
SC-DSA-30	17.1
SC-DSA-31	17.1

Table H-26. Depth sensitive areas and most depth sensitive areas 32–57 in Scotts Creek by river mile; bold rows with an asterisk (*) denote most depth sensitive areas.

Depth Sensitive Area Identifier	River Mile
SC-MDSA-32*	**17.1***
SC-MDSA-33*	**17.3***
SC-MDSA-34*	**17.3***
SC-DSA-35	17.4
SC-DSA-36	17.6
SC-DSA-37	17.6
SC-DSA-38	17.7
SC-DSA-39	17.7
SC-DSA-40	17.8
SC-DSA-41	17.9
SC-DSA-42	18.0
SC-DSA-43	18.0
SC-DSA-44	18.1
SC-MDSA-45*	**18.2***
SC-MDSA-46*	**18.2***
SC-DSA-47	18.5
SC-DSA-48	18.6
SC-DSA-49	18.6
SC-DSA-50	18.8
SC-DSA-51	18.8
SC-DSA-52	19.0
SC-DSA-53	19.1
SC-DSA-54	19.1
SC-DSA-55	19.2
SC-DSA-56	19.2
SC-MDSA-57*	**19.3***

Table H-27. Most depth sensitive areas 2–46 identified in Scotts Creek with simulated flows and depth outputs. Depths less than 0.5 ft are shown in bold marked with a hashtag (#) symbol.

Flow (cfs)	SC-MDSA-2	SC-MDSA-32	SC-MDSA-33	SC-MDSA-34	SC-MDSA-45	SC-MDSA-46
20	**0.32#**	**0.38#**	**0.41#**	**0.37#**	**0.24#**	**0.27#**
30	**0.38#**	**0.41#**	**0.49#**	**0.42#**	**0.27#**	**0.30#**
32	**0.39#**	**0.41#**	0.50	**0.43#**	**0.28#**	**0.30#**
40	**0.43#**	**0.43#**	0.56	**0.48#**	**0.30#**	**0.32#**
44	**0.47#**	**0.44#**	0.58	0.50	**0.32#**	**0.32#**
47	0.50	**0.45#**	0.60	0.52	**0.33#**	**0.33#**
50	0.53	**0.46#**	0.62	0.54	**0.34#**	**0.33#**
62	0.68	0.50	0.68	0.61	**0.42#**	**0.37#**
70	0.78	0.52	0.72	0.65	**0.47#**	**0.39#**
75	0.83	0.54	0.74	0.67	0.50	**0.41#**
88	0.97	0.59	0.80	0.73	0.57	**0.46#**
100	1.10	0.63	0.86	0.78	0.63	0.50
130	1.38	0.74	0.98	0.89	0.75	0.64
140	1.47	0.77	1.02	0.93	0.80	0.69

Table H-28. Most depth sensitive area 57 identified in Scotts Creek with simulated flows and depth outputs. Depths less than 0.5 ft are shown in bold and marked with a hashtag (#) symbol.

Flow (cfs)	SC-MDSA-57
20	**0.21#**
30	**0.25#**
32	**0.26#**
40	**0.28#**
44	**0.29#**
47	**0.30#**
50	**0.31#**
62	**0.34#**
70	**0.36#**
75	**0.37#**
88	**0.40#**
100	**0.42#**
130	**0.48#**
140	0.50

REFERENCES

Bovee, K. D. (1982). A guide to stream habitat analysis using the Instream Flow incremental methodology. Instream Flow and Aquatic Systems Group, Western Energy and Land Use Team, U.S. Fish and Wildlife Service, Fort Collins, CO. Instream Flow Information Paper: No. 12.

Bray, D. I. (1979). Estimating average velocity in gravel-bed rivers. American Society of Civil Engineers **105**(No. HY9): 1103–1122.

BV EPA (2023). Adobe Creek *chi* habitat suitability assessment. Big Valley Band of Pomo Indians Environmental Protection Agency (BV EPA). Available: https://www.bvrancheria.com/_files/ugd/f2d74c_dc382f74eb164efd90495da5811ee481.pdf.

CDFW (2020). Standard operating procedure for discharge measurements in wadeable streams in California. California Department of Fish and Wildlife, Instream Flow Program (CDFW), West Sacramento, CA. CDFW-IFP-002, version 2. Available: https://nrm.dfg.ca.gov/FileHandler.ashx?DocumentID=74169.

CDFW (2023). Instream Flow Program quality assurance plan. California Department of Fish and Wildlife, Instream Flow Program (CDFW), West Sacramento, CA.

Chow, V. T. (1959). Open-channel hydraulics. In. McGraw-Hill, NY. pp. 680.

Cowan, W. L. (1956). Estimating hydraulic roughness coefficients. Agricultural Engineering **37**(7): 473–475.

Kinzel, P. J., C. J. Legleiter and J. M. Nelson (2012). Mapping river bathymetry with a small footprint green LiDAR: applications and challenges. Journal of the American Water Resource Association **12**: 1–22.

NV5 (2024). Clear Lake tributaries, Lake County, California 2024 topobathymetric lidar technical data report. CDFW, Corvallis, OR.

USACE (2025). HEC-RAS version 6.2 user's manual. USACE Hydrologic Engineering Center, Davis, CA. Available: https://www.hec.usace.army.mil/confluence/rasdocs/rasum/6.5.

USFWS (2011). Sacramento Fish and Wildlife office standards for physical habitat simulation studies. U.S. Fish and Wildlife Service, Sacramento Fish and Wildlife Office, Restoration and Monitoring Program (USFWS), Sacramento, CA.

Wolman, M. G. (1954). A method of sampling coarse river-bed material. Transactions of American Geophysical Union **35**(6): 951–956.

WVDEP (2025). Pebble count methods. West Virginia Department of Environmental Protection Watershed Improvement Branch, Charlston, WV. Accessed: May, 2024.